DOE/NASA/0030–9
NASA CR–190772

Tribological and Microstructural Investigation of the PM200 Series of Self-Lubricating Composites

Michael S. Bogdanski
Case Western Reserve University

November 1992

Prepared for
NATIONAL AERONAUTICS AND SPACE ADMINISTRATION
Lewis Research Center
Under Contract NCC 3–30

for
U.S. DEPARTMENT OF ENERGY
Energy Conservation and Utilization Technologies

DOE/NASA/0030–9
NASA CR–190772

Tribological and Microstructural Investigation of the PM200 Series of Self-Lubricating Composites

Michael S. Bogdanski
Case Western Reserve University
Cleveland, Ohio 44106

November 1992

Prepared for
National Aeronautics and Space Administration
Lewis Research Center
Cleveland, Ohio 44135
Under Contract NCC 3–30

for
U.S. DEPARTMENT OF ENERGY
Energy Conservation and Utilization Technologies
Washington, D.C. 20545
Under Interagency Agreement DE–A101–91CE50306

TRIBOLOGICAL AND MICROSTRUCTURAL INVESTIGATION OF THE PM200 SERIES OF CHROMIUM CARBIDE-BASED SELF-LUBRICATING COMPOSITES

Michael Scott Bogdanski
Case Western Reserve University
Cleveland, Ohio 44106

SUMMARY

This master's thesis describes an investigation of the effects of processing and compositional variations on the tribological, microstructural, and compressive strength characteristics of PM212. PM212 is a self-lubricating composite, comprised of a wear resistant metal bonded chromium carbide matrix, containing the solid lubricants barium fluoride/calcium fluoride eutectic and silver. Several alternate composites were formulated which had lubricant and matrix variations. Processing variations included sintering and hot isostatic pressing (HIPping). Pin-on-disk tests were used to screen the alternates for friction and wear properties. Several of the chromium carbide-based self-lubricating composites exhibited low friction and wear in sliding against a nickel-based superalloy. One specific composition contained gold in place of silver to minimize the potential reactivity of the composite with possible environmental contaminants such as sulfur. This formulation also resulted in a composite with good tribological properties. The results indicate that several of these composites have potential use as sliding bearing and seal materials in operation from 25°C to temperatures as high as 900°C. The good tribological performance by several different composites showed that the composition of PM212 can be altered without dramatically affecting performance.

CHAPTER 1

INTRODUCTION

There is an ongoing need for materials which can be used for sliding bearings and seals requiring operation from below room temperature to temperatures as high as 900°C in oxidizing, reducing, and inert atmospheres. Oil lubrication cannot be used to cover the temperature range in these applications since the upper limit of oil lubricants is 300 to 350°C (Reference 1). Solid lubricants offer the potential to meet these lubrication challenges. However, the traditional solid lubricants such as molybdenum disulfide (MoS_2) and graphite do not have the temperature capabilities needed.

Traditional solid lubricants such as graphite, MoS_2, and polytetrafluoroethylene (PTFE) function well within certain regimes (Reference 2). PTFE lined bearings provide exceptionally low friction but have an upper temperature limit of approximately 150°C. Above this temperature, the PTFE softens and wear increases considerably (Reference 2). MoS_2 is an excellent solid lubricant for vacuum applications from low temperature up to 650°C. However, in air, MoS_2 oxidizes to form molybdic oxide (MoO_3) which does not provide lubrication. This oxidation occurs at temperatures as low as 300°C, and is very dependent on the flow rate of oxygen to the compound (Reference 2). Graphite does not perform well in vacuum or in dry air because its ability to lubricate relies on the absorption of moisture and hydrocarbons. The maximum service temperature for lubrication by graphite is approximately 550°C, beyond which, severe oxidation inhibits its lubrication ability and life (Reference 2).

The limitations of the traditional solid lubricants underscore the need for innovative material systems capable of providing lubrication over a wide range of

temperatures. In addition, these systems must be able to withstand corrosive atmospheres. The PS200 and PM200 composites have been developed at NASA Lewis Research Center in response to these needs.

The PS200 plasma sprayed composite coating series and the PM200 series of powder metallurgy composites have been shown to provide low friction and wear over a wide temperature spectrum. PS200 and PM200 composites are comprised of a wear resistant metal bonded chromium carbide (Cr_3C_2) matrix with the solid lubricants barium fluoride/calcium fluoride (BaF_2/CaF_2) eutectic and silver. Silver is present as a low temperature lubricant (up to 500°C). The BaF_2/CaF_2 eutectic functions as the high temperature lubricant (400°C and up). The solid lubricant additions provide lubrication by forming a low shear strength film during sliding. The eutectic is used instead of a single fluoride since it has a lower melting point and thus a lower softening temperature. The composite materials function by replenishing the sliding contact surfaces with lubricants as wear occurs. In doing so, a film containing the low shear strength lubricants is formed at the sliding interface (Reference 3).

Potential applications for these materials include cryogenic process control valves, variable temperature control surface bearings, high temperature combustion engine cylinder wall coatings, backup lubricant coatings for gas bearings, and turbine engine seals and bushings (References 4-6).

Research at NASA Lewis Research Center which led to this thesis essentially began with an investigation of the feasibility of using solid fluorides as a lubricant in 1960 (Reference 7). This work focused on the lubricating properties of ceramic coatings, diffusion-bonded fluoride coatings, and ceramic-bonded fluoride coatings to temperatures as high as 815°C. Promising results were obtained with ceramic-bonded CaF_2 coatings. Thin films of CaF_2 applied to the surface of the ceramic-bonded coatings further improved lubrication. However, the thin film coatings only performed well above 400°C and had a limited life.

This was followed throughout the next twenty-five years by several studies of various high-

temperature and low-to-high temperature, self-lubricating coating and composite systems. Additionally, different methods of applying coatings and making composites were investigated. One system used porous Inconel (a nickel-based superalloy) infiltrated with fluorides (Reference 8). This had a long life compared to the thin films, but still had a minimum useful temperature of 400°C. Another system was a thin fluoride coating which contained MoS_2 (Reference 9). This had a useful temperature range of 25°C to 800°C, however, the MoS_2 oxidized at the higher temperatures. Hence, the coating was ineffective at lower temperatures once the MoS_2 was oxidized. Silver was also incorporated into thin fluoride coatings (Reference 9) to aid in the lubrication at lower temperatures. In addition, silver has a high melting point (961°C) and is relatively non-oxidative, with the exception of a light oxide formation between 200°C and 300°C. Beyond 300°C, the oxide reduces to elemental silver (Reference 10). This silver containing fluoride coating had a wide temperature range, yet still possessed a limited due to its limited thickness. Following this work, metal binders with an anti-oxidant glass were incorporated into the silver-fluoride coatings, using plasma spraying techniques (Reference 11). This system had a wide temperature range capability and a longer life due to its increased thickness, but still had an inadequate wear resistance for long duration applications.

In 1985, the use of silver and fluorides as lubricants in a nickel-cobalt (NiCo) bonded chromium carbide-based plasma sprayed coating was studied in both pin-on-disk and gas foil bearing tests (References 12,13). It was observed that thick films of silver alone did not function well due to the excessive plowing which occurred (Reference 12). Thus, the silver would only function well as a thin film if used by itself. However, a composite of silver with a wear resistant matrix material would eliminate the plowing effect encountered in a silver film alone. Additionally, solid fluorides were added based on the previous knowledge of their ability to lubricate at higher temperatures. The foil bearing and pin-on-disk tests indicated that the PS200 coating (80wt% NiCo-Cr_3C_2, 10% Ag, and 10% BaF_2/CaF_2 eutectic) provided lower friction and wear than the unmodified NiCo-Cr_3C_2 coating (Reference 13). This ternary system concept was an outgrowth

of the work in Reference 11 which used metal alone as the wear resistant matrix for the dispersed solid lubricants.

Several studies performed from 1985 to 1990 are reported in References 3, 14-18, wherein detailed research programs were conducted to further investigate self-lubricating, wear resistant, plasma sprayed composite coatings. Two of the programs focused on the refinement of the plasma sprayed coating composition; one with gas-foil bearing studies (Reference 18) and the other with pin-on-disk studies (Reference 3).

The silver and fluoride lubricants were found to behave synergistically, i.e., the performance of the coating decreased when only one of the lubricants was present. The effect of atmosphere on the tribological performance was investigated in Reference 14. It was found that the best performance occurred in a hydrogen atmosphere. Both friction and wear increased in an oxidizing atmosphere (air). Silver films (100 to 150nm thickness) sputtered onto the PS200 coating provided a beneficial effect by enriching the surface with lubricant and reducing the initial abrasiveness of the ground PS200 surface (Reference 15). This in turn reduced the initial wear of the counterface pin in the pin-on-disk test.

The quality control requirements of the PS212 coating (70wt% NiCo-Cr_3C_2, 15% Ag, and 15% BaF_2/CaF_2 eutectic) were investigated in Reference 16, wherein optimum parameters were determined for machining techniques, plasma spraying, and heat treatment. Limitations of plasma spraying, such as the difficulty associated with inside diameter coating and waste associated with over-spray led to the development of a powder metallurgy version of PS200, namely, PM212.

In 1990, the tribological properties of PM212 (70wt% NiCo-Cr_3C_2, 15% Ag, and 15% BaF_2/CaF_2 eutectic) pins in sliding against superalloy disks were reported in Reference 19. The PM212 pins were fabricated by the use of cold compaction techniques followed by pressureless furnace sintering. The composite pins were tested over a spectrum of temperatures, sliding velocities, and applied loads and were found to exhibit good tribological properties. Mechanical and thermophysical properties of PM212 were then investigated (Reference

20).

It was found that fully dense PM212 formed by hot isostatic pressing (HIPping) was three times stronger in compression than sintered PM212 which was only 78% dense. Several other properties including tensile strength, elastic modulus, thermal expansion coefficient, and thermal conductivity were determined. Most recently, a comparison of the tribological performance of sintered PM212 and HIPped PM212 showed that the HIPped version provided slightly lower friction and wear (Reference 21). Finally, the effects of replacing the silver in PM212 with gold, which represents a portion of this thesis, is also detailed in Reference 22.

The plasma sprayed and powder metallurgy composites described herein are protected by U.S. Patents 4,728,488 and 5,034,187 (References 23,24). These patents cover the general concept of the carbide/fluoride/silver composites, including both composition and manufacturing methods.

This present investigation focuses on the effect of processing and compositional changes on the performance of the PM212 powder metallurgy high temperature self-lubricating composite. Figure 1.1 illustrates the approach utilized in this investigation, which will be detailed in the remainder of this chapter. Alternate compositions chosen for study had unique characteristics, such as matrix only (no added lubricants), only a single lubricant added, single fluoride in place of the eutectic fluoride, additional amount of lubricant, added unbonded chromium carbide in place of some of the metal bonded chromium carbide, and the use of gold instead of silver.

A tribological evaluation of the alternate compositions was performed at several temperatures using pin-on-disk methods. Two processing routes were used in this investigation; cold compaction followed by sintering and cold compaction followed by HIPping. HIPping yields parts of higher strength and density in comparison to sintering (Reference 20). Hemispherically tipped pins fabricated from the composites were slid against nickel-based superalloy disks in a pin-on-disk tribometer with temperatures ranging from 25 to 900°C at a sliding velocity of 2.7m/s. The intent of the evaluation was to determine if any of the processing or compositional changes had

a substantial positive or negative effect on tribological properties.

The silver in PM212 imposes certain limitations on the use of the composite. Silver has the lowest melting point of the constituents of the composite (961°C). Thus, the material cannot be used much above 900°C. Additionally, silver combines directly with sulfur (a constituent typically found in petroleum derived fuels) to form silver sulfide (a corrosive compound), even at low temperature (Reference 10). The possibility for stress corrosion cracking of superalloys due to sulfidation attack is a concern.

Since intended applications of PM212 are in turbine engines which use superalloys, it is desirable to have a composite which does not contain an easily sulfided element, such as silver. Hence, a portion of this study investigates the feasibility of replacing the silver in PM212 with the volumetric equivalent of gold. The new composite is designated PM212/Au and has the following composition: 62wt% NiCo-Cr_3C_2, 25% Au, 13% BaF_2/CaF_2 eutectic.

Gold in its metallic state does not combine directly with sulfur (Reference 10). Thus, the potential for sulfide formation with the low temperature lubricant in the composite is eliminated. In addition, by replacing the silver with gold (melting point, 1063°C), the eutectic has the lowest melting point (1050°C). Hence, the upper temperature limit for the composite may be higher than 900°C for limited periods.

The HIPped gold-containing composition PM212/Au and HIPped PM212 were further studied over a wide range of sliding velocities (0.27m/s to 10.0m/s) using pin-on-disk methods at temperatures from 25°C to 900°C. Repeatability trends were determined by performing several pin-on-disk tests under similar conditions.

Since the PM212/Au composite has intended uses in turbines which may employ low speed bushings, very low velocity (0.027m/s) pin-on-disk tests were used to simulate these conditions. Tests were conducted at temperatures ranging from 25°C to 760°C at the 0.027m/s velocity.

Analytical methods such as scanning electron microscopy (SEM), energy dispersive x-ray

spectroscopy (EDS), and optical microscopy were employed for analysis of wear surfaces. In addition, the composite microstructures were compared using optical microscopy, SEM, EDS, and density measurement.

CHAPTER 2

MATERIALS AND PROCESSING

Materials and Processing Selection

The purpose of this investigation was to study the effects of composition and processing changes on the performance of self-lubricating powder metallurgy composites. The different processing routes used were cold compaction followed by sintering and cold compaction followed by hot isostatic pressing. Figure 2.1 contains a schematic of the processing routes used, which are further detailed in this chapter.

Ten different compositions were formulated for this investigation. Table 2.1 summarizes the reasons for choosing each of the compositions for this study. The PM212 composition (70wt% 430NS, 15% Ag, 15% BaF_2/CaF_2 eutectic) is the baseline composition which has previously been studied in both plasma sprayed and powder metallurgy forms as described in Chapter 1. The 430NS functions as the wear resistant base material and was tested alone to determine the effect of no added lubricants. The 430NS+Ag and 430NS+Eut were chosen to examine the single lubricant condition. PM212/Au was the same composition as PM212 with the silver replaced by the volumetric equivalent of gold. PM212/BaF_2 and PM212/CaF_2 were formulated to study the effect of the single fluorides in place of the eutectic fluoride. PM226 had additional silver added to determine the effect of added lubricant. Finally, PM221 and PM225 had Cr_3C_2 with no binder metal incorporated, substituted in place of some of the metal bonded Cr_3C_2. This was to determine if the harder non-metal bonded chromium carbide would improve the wear resistance of the composite.

Powders and Preparation

The powders used to make the self-lubricating composites are commercially available from several sources. The powders used for this investigation were obtained from the following sources: 430NS from Metco, silver from Degussa, gold from Leach and Garner, barium fluoride and calcium fluoride from Fisher Scientific, and chromium carbide from Sulzer Plasma.

The BaF_2/CaF_2 eutectic is a 62/38wt% blend. The eutectic was formed by prefusing the mixed fluorides in a nitrogen atmosphere at 1100°C. Then , the eutectic was crushed, and ball milled to produce a fine powder size for use in the composites. This process is fully described in Reference 17.

The 430NS is a nickel-cobalt bonded chromium carbide powder. Table 2.2 lists the composition of 430NS based on manufacturer's literature. Table 2.3 contains the sieve ranges and purity levels for the powders used.

The powders were weighed and combined in the proportions listed in Table 2.4 for each composition. Each combined batch of powder was loaded into a V-type mixer and blended for 30 minutes to produce a uniform distribution of the different powders. After blending, the batches were then ready for processing into the desired shapes using the powder metallurgy techniques to be described.

Cold Compaction

Cylindrical slugs (13mm diameter by 32mm long) were formed by a die press followed by cold isostatic pressing. The blended powder was poured into a steel die lined with graphite sheet foil. An axial load of 35.6kN was applied which generated a pressure of approximately 281MPa (41ksi) on the powder in the die. The die pressed cylindrical slugs were then placed in rubber bags. The bags were placed in a chamber which was pressurized to 414MPa (60ksi) for 5 minutes. The specimens were removed from the pressure chamber and then the slugs were removed from the rubber bags. This rubber bag-pressure chamber method is the cold isostatic

pressing (CIPping) technique. This two stage compaction scheme yielded slugs with a green densities ranging from 70 to 80%.

Pressureless Sintering

The CIPped specimens were placed into a tube furnace with a dry hydrogen atmosphere, which was used to prevent oxidation of the specimens during the sintering process. The furnace was heated at a rate of 10°C/min up to 1100°C, and then held at temperature for 30 minutes. The furnace was then cooled at a rate of 10°C/min down to room temperature before the specimens were removed.

Hot Isostatic Pressing

The CIPped specimens were placed into stainless steel cans lined with graphite sheet foil. The unsealed cans were vacuum annealed at 350°C. After annealing, the cans were vacuum sealed using electron beam welding. The sealed cans were placed into a chamber that was simultaneously pressurized and heated. The chamber was heated to 1100°C at a rate of 6°C/min and pressurized with argon to 138MPa (20ksi) at a rate of 0.75MPa/ min. The chamber was held at 1100°C and 138MPa for 20 minutes. Then, the chamber was cooled at a rate of 12°C/min and depressurized at a rate of 1.5MPa/min. The specimens were removed from the chamber and then the slugs were removed from the cans.

Superalloy Disks

The disk specimens used for the pin-on-disk testing were made of the nickel-based superalloy René 41. René 41 has excellent high temperature oxidation resistance and strength and is a commonly used aerospace material. Table 2.5 lists the composition of René 41. Nickel makes up approximately 55wt% of the alloy, with chromium, cobalt, and molybdenum as secondary

constituents. Several trace elements are present in the alloy. René 41 is precipitation hardened to a nominal hardness of Rockwell "C" 35-40 at room temperature.

Machining Techniques

The cylindrical slugs produced from both the CIP-sinter and CIP-HIP routes were fabricated into hemispherically tipped pins. The slugs were centerless ground to obtain a cylindrical diameter of 9.53mm. The nominal pin length was approximately 30mm. 4.76 mm hemispherical radii were placed on both ends of the pins using diamond grinding. The diamond grinding technique is used to prevent the softer phases (silver and fluorides) from being selectively removed from the hemispherical surface (Reference 16). In addition, only clean water is used as a coolant. Machining oils are not used so that contamination of the composite is minimized.

Specimens were also made into small right circular cylinders and rectangular blocks to allow for density determination by weight and measure. Additionally, small cylindrical pins (5mm in diameter and 10mm in length) were made of the sintered composites for compressive strength testing.

The superalloy disks were machined using standard techniques. The fabricated disks had a diameter of 63.5mm and a thickness of 12.7mm. After machining to size, the disks were lapped to an average surface roughness of 400Å center line average (CLA).

Metallographic Preparation

Cross sections of the powder metallurgy composites were prepared by mounting the samples in epoxy. The mounted samples were diamond sawed to expose the cross section of the composite. The cut surface was then diamond polished using a sequentially finer grit to a final paste grit size of 0.5μm.

CHAPTER 3

EXPERIMENTAL AND ANALYTICAL METHODS

Specimen Preparation for Pin-on-Disk Testing

The composite pins were vacuum heated for 3 hours at 200°C and 60 torr (air atmosphere) to remove any residues from the processing, handling and machining operations. The pins and disks were then cleaned with ethyl alcohol, wet scrubbed with 0.1μm grit size alumina powder, rinsed with distilled water, and dried with compressed air.

Pin-on-Disk Rigs

Two different pin-on-disk tribometers were used for this study. One which uses an induction coil for specimen heating was used to perform the 2.7m/s, 0.27m/s, and some of the 0.027m/s tests (Figure 3.1). The surface temperature of the disk specimen was measured with an infrared pyrometer and a continuous readout of the friction force was made on a chart recorder from a temperature compensated strain gage bridge transducer. The second tribometer, used for the 10.0m/s and some of the 0.027m/s tests incorporated a resistance heated furnace (Figure 3.2). This rig is fully described in Reference 25. A computerized data acquisition system monitored test conditions such as normal load force, friction force, and furnace temperature. The normal load force and friction force were also recorded on a chart recorder for comparison to the computer acquired data.

Tribological Evaluation of Alternates

Pin-on-disk tests were performed at a sliding velocity of 2.7m/s at temperatures of 25°C, 350°C, 760°C, and 900°C. The composite pins were slid

against the René 41 superalloy disks. A new set of specimens (new pin and new disk) was used for each temperature. The test load was 4.9N and the atmosphere was air with relative humidity of 35% at 25°C. The 4.9N load was chosen to facilitate comparison with previous work (References 19, 21) and is considered a typical load for sliding bearing and seal applications.

One test was performed for a duration of 70 minutes at each temperature for each sintered and HIPped composite. For the sintered alternates at 25°C and 350°C, the 70 minute tests were split into segments of 10-20-40 minutes.

Further Comparison of HIPped PM212 and PM212/Au

HIPped PM212 and PM212/Au pins were slid against René 41 superalloy disks at sliding velocities from 0.27 to 10.0m/s. The test load was 4.9N, the atmosphere was air with relative humidity of 30 to 70% at 25°C, and the temperature range was 25 to 900°C. Table 3.1 lists the test combinations (speed-temperature-time) performed for this study.

Additionally, two studies were performed to determine run-in effects on wear at the 2.7m/s sliding velocity. For PM212/Au, a series of brief tests were performed at 25°C and 2.7m/s. The durations were 1 and 10 minutes with two tests performed at each condition. New specimens were used for each test. Pin wear and disk wear were measured for comparison with longer duration tests. For PM212, pin wear was measured after 10, 30, and 70min for the same set of specimens. This procedure was performed at 25, 350, and 760°C. A new set of specimens was used for each temperature.

Low Speed Investigation of PM212/Au

The PM212/Au composition was slid against René 41 at a velocity of 0.027m/s, with temperatures ranging from 25°C to 800°C. The test durations ranged from 70 minutes to 88 hours. The effects of run-in at higher speeds (0.95 to 2.7m/s) previous to sliding at 0.027m/s were

studied.

Wear Determination and Wear Factors

Both tribometers generate 51mm diameter wear tracks on the rotating disk while holding the pin in a fixed position. After the test run, a photomicrograph is taken of the pin wear scar to determine the volume removed. A stylus surface profilometer is used to measure the wear track profile on the disk. Typically, four measurements of the wear track area are averaged. The area of the wear track is multiplied by the track circumference to determine the wear volume. Figure 3.3 shows a pin wear scar and a disk wear track profile scan for one of the tests performed.

Wear factors were computed for both the pin (K_{pin}), and the disk (K_{disk}). Where several tests were performed, an average wear factor was determined with a standard deviation representing the test to test scatter. Wear factors are further detailed in Appendix A. Briefly, the wear factor is equal to the volume removed due to wear during sliding divided by the product of the normal load and the total sliding distance. Wear factors higher than $10^{-4}mm^3/N\text{-}m$ are considered unacceptably high for most applications and those less than $10^{-6}mm^3/N\text{-}m$ are considered very low.

Friction Data Analysis

The friction coefficient is determined by dividing the measured frictional (tangential) force by the normal load force on the pin. The average coefficient of friction, μ, for each test run is determined by averaging a sampling of data points recorded throughout the test. A sample standard deviation about this average, $s(\mu)$ represents the typical scatter that was present in the test. When five or more tests were run at similar conditions, an overall average coefficient of friction is computed, and the standard deviation about the overall average represents the test to test variation.

Wear Surface Analysis

Wear surfaces of the pin and disk were analyzed using optical microscopy, SEM, and EDS. The disk wear tracks were examined for transfer films formed from sliding against the composite pins. Additionally, the surface morphology of the wear tracks were examined. Settings used on the SEM were 20kV accelerating voltage, 6.0×10^{-10}Å probe current, and 39mm working distance. Optical microscopy was used to observe general features of the wear surfaces at low magnification.

Microstructural

Metallographically polished surfaces of the composites were examined using optical microscopy, SEM, and energy dispersive x-ray spectroscopy (EDS). The EDS system is an integrated part of the SEM. The analyses helped to compare and characterize the microstructures based on elemental distribution and surface topography.

Settings used on the SEM were 20kV accelerating voltage, 6.0×10^{-10}Å probe current, and 39mm (15mm for backscatter) working distance. The backscattering mode of the SEM was used to illustrate the elemental distribution differences. Brighter areas correspond to higher atomic number elements. Key elements were identified using x-ray mapping with the EDS system. The SEM work was performed at several magnifications. Optical micrographs of the composites were obtained using vertical illumination on a metallographic microscope at several magnifications.

Density Measurement

The densities of the alternate compositions in both HIPped and sintered forms were determined by weight and volume measure. Measured density was compared to theoretical density to determine the porosity level present after processing. Density and porosity levels of PM212 have previously been established using liquid porosimetry and weight and measure techniques

(Reference 20).

Compressive Strength Determination

Compression tests were performed using cylindrical specimens of the sintered alternates. The tests were conducted at 25°C, 350°C, 760°C, and 900°C in air on a load testing rig at a strain rate of 2.1×10^{-4} s^{-1}. Three tests were performed at each condition. The compression tests of the sintered alternates were performed in conjunction with the work of Reference 20. Reference 20 contains complete experimental techniques for the compressive strength measurements, and the methodology for determining 0.2% offset yield strength.

CHAPTER 4

RESULTS

Tribological Evaluation of Alternates

The average friction coefficients for the sintered alternates and the HIPped alternates are summarized in Table 4.1. The standard deviations about the averages are also included. These friction coefficients and deviations were obtained from the 70 minute test performed on each composite. The results show that the average friction coefficient ranged from 0.16 to 0.44.

Tables 4.2 and 4.3 summarize the pin wear factors (K_{pin}) and disk wear factors (K_{disk}), respectively, for the sintered and HIPped alternates. These wear results correspond to the frictional results above. K_{pin} ranged from $3.9 \times 10^{-7} mm^3/N\text{-}m$ to $1.7 \times 10^{-4} mm^3/N\text{-}m$. K_{disk} ranged from -2.9×10^{-5} $mm^3/N\text{-}m$ to $6.7 \times 10^{-5} mm^3/N\text{-}m$ (negative wear factor indicates buildup).

Since only one 70 minute test was performed at each temperature for each composite, the test-to-test variation for a specific composite at a given condition cannot be stated. However, from the tests performed, overall performance across the temperature range can be compared. Table 4.4 shows how the composites ranked in overall friction coefficient relative to one another. The PM226 sintered alternate, which contained additional silver compared to the baseline PM212, had the lowest overall average friction coefficient (0.31) of the sintered alternates. Sintered PM212 had the highest overall average friction coefficient (0.38) of the sintered alternates. The HIPped 430NS+Ag composite had the lowest overall average friction coefficient (0.25) of the HIPped composites. The HIPped PM212/CaF_2 had the highest overall average friction coefficient (0.33) of the HIPped composites.

These rankings were also made for pin wear and disk wear and are summarized in Table 4.5 and Table 4.6 respectively.

Figure 4.1 illustrates the run-in behavior of the sintered alternates at room temperature. This includes both the composite pins and the René 41 disks. The plots show a slight decline in wear factor with sliding distance. This decline is slightly more pronounced for the disk than for the pin.

Microstructural and Mechanical: Alternates

Figure 4.2 contains optical micrographs of all of the composites, both sintered and HIPped, studied in this investigation. The scale is the same for all of the microstructures shown (as labeled on the images). The dark features correspond to eutectic and pore space (Reference 19). The brightest areas correspond to silver deposits, and the middle gray is the 430NS (and non-metal bonded chromium carbide in PM221 and PM225).

The presence or absence of pore space was determined by measuring the density. Table 4.7 contains the theoretical and measured densities for the composites by both sintering and HIPping. The percent of theoretical density achieved ranged from 52.9% (430NS) to 81.8% (PM226) for the sintered alternates. Every composition except PM212/Au, the gold containing composition, HIPped to full density. The residual porosity in PM212/Au from HIPping will be further discussed in the section comparing HIPped PM212 and HIPped PM212/Au. The microstructure of HIPped PM212/CaF_2 appeared differently than that of HIPped PM212/BaF_2 (Figure 4.2) perhaps due to the higher melting point of CaF_2 (melting points: BaF_2, 1280°C; CaF_2, 1360°C).

Table 4.8 summarizes 0.2% offset compressive yield strength results obtained for the sintered alternates at the four temperatures investigated. In general, the strength decreases with increasing temperature. Figure 4.3 is a plot of the 0.2% offset compressive yield strength versus percent residual porosity after sintering. The plot contains strength data at 25°, 350°C, and 760°C.

The strength decreases as residual porosity level increases. The strength data at 900°C were all very low and do not clearly correlate with residual porosity level.

HIPped PM212 and PM212/Au Comparison: Tribological

Table 4.9 summarizes the friction coefficients and the pin and disk wear factors for the HIPped PM212 and PM212/Au composites at the speed-temperature combinations studied. For the 2.7m/s speed, five to six tests at each speed-temperature combination were performed. Thus, the friction coefficients and wear factors represent the overall averages.

Figure 4.4 contains plots of friction coefficient versus temperature for the three test speeds. Error bars (one standard deviation in each direction) for PM212 at the 2.7m/s speed are based on the test to test variation, whereas all others are based on the variation within a single test. The dashed lines are present to suggest a trend and aid in visualizing the relationship between the data points. Tests were not performed at intermediate temperatures. The friction coefficient was typically between 0.25 and 0.4 (Figure 4.4). PM212 at 0.27m/s and 25°C was the exception with a friction coefficient of 0.5. In several cases, the friction coefficients of the two composites were within data scatter of each other.

Plots of K_{pin} versus temperature for the three test speeds are found in Figure 4.5. The wear factor is plotted on a log scale. The pin wear behavior for the two composites were similar to each other except at the 10.0 and 2.7m/s tests where at higher temperature, the pin wear for PM212/Au was notably higher than that of PM212. The pin wear was typically in the low $10^{-5}mm^3$/N-m range, with a few cases in the low $10^{-6}mm^3$/N-m range. K_{pin} for PM212/Au at elevated temperature-higher speed conditions was high $10^{-5}mm^3$/N-m. A notable reduction in K_{pin} occurred at 760°C, 0.27m/s speed to low $10^{-6}mm^3$/N-m (Figure 4.5).

Several cases produced a "positive" disk wear. That is, a transfer from the pin to the disk caused a buildup on the disk. Table 4.9 indicates at which cases this occurred by the negative sign. K_{disk} was low $10^{-5}mm^3$/N-m or less except for the 0.27m/s tests where the disk wear

exceeded $1x10^{-4}mm^3/N-m$ in a few cases.

The results of the run-in study for PM212 are plotted in Figure 4.6. At 25°C and 350°C, the pin wear factors were nearly constant at 1 to $2x10^{-5}mm^3/N-m$. K_{pin} decreased at 760°C from $1x10^{-6}mm^3/N-m$ at 20min to $5x10^{-7}mm^3/N-m$ at 70min. This indicated that the run-in process was essentially completed within the first ten minutes. Figure 4.6 shows that higher wear (both pin and disk) occurred in the initial sliding for PM212/Au. The one minute test revealed a wear factor of approximately $1x10^{-4}mm^3/N-m$ for both the pin and disk. The ten minute test revealed wear factors in the low $10^{-5}mm^3/N-m$ range. The pin and disk wear factors further decrease as the 70min data points illustrate. A run-in mode with higher wear was observable with the one minute test. This run in was also observable in the friction behavior. Friction was typically higher during the initial two minutes of sliding then decreased to the steady state value.

HIPped PM212 and PM212/Au Comparison: Microstructural

The theoretical densities of PM212 and PM212/Au are 6.61 and $7.48g/cm^3$ respectively. PM212 achieves near full density, with a remaining porosity of 0.2%. PM212/Au achieved a density of $6.34g/cm^3$, with a remaining porosity of 15.2%.

Figure 4.7 contains micrographs obtained with the SEM. The backscatter images present an elemental view of the composites. To identify the major components, x-ray mappings of nickel, chromium, barium/calcium, silver for PM212, and gold for PM212/Au were obtained. The mappings show a similar distribution of the major components for the two composites.

Figure 4.8 contains low magnification optical and high magnification SEM (secondary electron image, SEI) micrographs of the two composites. The main observation regarding the optical micrographs is that PM212/Au contains a greater percent of dark area (pore space and eutectic). Distinct pores in the PM212/Au microstructure are clear in the SEM image. The distinct

pores in PM212/Au were discernable due to the depth of field possible with the SEM. Since the two composites had the same volumetric percentage of eutectic, PM212/Au possesses more pore space than PM212. An examination of PM212 at higher magnification revealed only minute pores in comparison to those observed at higher magnification in PM212/Au. At higher magnification on the optical microscope, the gold appeared as an interconnected, fine web-like structure whereas the silver appears in distinct pockets. A subtle shade difference between the gold and the carbide matrix made reproduction of the micrograph for illustration impractical.

The gold powder particle cross sections were examined for structure and morphology. They were found to be solid as seen from the cross section micrograph in Figure 4.9. Figure 4.9 also includes samples of the starting silver and gold powders. It is noted that the predominant size of the silver was near the high end of the sieve range (≈150μm) whereas the predominant size of the gold was near the low end (≈50μm).

Low Speed HIPped PM212/Au

The PM212/Au composite was tested at a very low speed (0.027m/s) to better simulate a low speed bushing. Initially, a 70 minute test was performed at 25°C, 350°C, and 760°C, using a new set of specimens for each temperature. The resulting friction coefficients were high compared to tests performed at the other speeds. Notably, the test at 25°C yielded a friction coefficient of 0.7. The friction coefficient was lower at 350°C (0.39). However, at 760°C, the friction coefficient was higher again (0.48). Since the friction coefficients at 25°C and 760°C were unusually high, retests were performed. In the retests, a run-in period (70 minutes) at a higher sliding velocity (0.95m/s) was employed. After the higher velocity run-in, the specimens were then run at the 0.027m/s velocity for 70 minutes. During the 0.027m/s portion, friction coefficients of 0.25 and 0.27 resulted at the 25°C and 760°C tests, respectively. The resulting friction coefficients were much lower than the ones previously encountered.

The disk wear tracks were analyzed using the SEM/EDS system to determine reasons for

the frictional behavior during these tests. Figure 4.10 contains micrographs obtained on the SEM of the wear tracks from the 25°C (no run-in), 25°C (run-in) and 350°C tests. The wear track from the 25°C test where no run-in period was employed contains little evidence of transfer films formed from sliding against the PM212/Au pin. However, regions of transfer films are evident in the wear track from the 25°C test which employed the higher velocity run-in. The micrograph from the 350°C test shows patches of transfer also. EDS spectra from the wear tracks of these three tests are plotted in Figure 4.11. The spectrum for each test is the average of spectra obtained from 3 locations, 120° apart in the wear track. The spectra are essentially identical, showing very little deviation. This illustrates that the frictional behavior was not caused by chemical and/or compositional differences of the various wear tracks.

Figure 4.12 contains optical micrographs of the pin scars and SEM micrographs of the disk wear tracks from the 760°C tests. The initial test which employed no run-in shows a white substance on the pin scar. The wear track corresponding to this test shows a film which appears to have melted and re-solidified. This heavy film on the pin and the disk is composed primarily of the BaF_2/CaF_2 eutectic. The test which employed a higher velocity run-in period does not show this heavy fluoride buildup on the pin or disk wear surfaces. The wear track does show patches of transfer from the PM212/Au pin. The EDS spectra (obtained similarly as described above) for these two tests are compared in Figure 4.13. The two spectra are clearly different. The spectra corresponding to test with no run-in shows the presence of the fluoride buildup, as seen by the strong Ba and Ca peaks. Additionally, the nickel peak was sharply reduced in this case. The spectrum from the test which employed the run in appeared very similar to the spectra from the 25°C and 350°C tests (Figure 4.11).

Several other tests were performed to further understand the behavior of PM212/Au at the sliding velocity of 0.027m/s. The friction and wear results from these tests, as well as the tests detailed above are summarized in Table 4.10. The most notable result is that a friction coefficient of 0.1 was obtained at 25°C after a long duration of sliding. This was producible both with

elevated velocity run-in and no run-in. It appeared that approximately 1-2km of sliding at 0.027m/s was required to produce this effect. A film of gold completely covering the wear scar was visible on the pin after the tests where the 0.1 friction coefficient occurred.

CHAPTER 5

DISCUSSION

Alternates Evaluation

There was considerable overlap in the overall rankings for friction coefficient, K_{pin}, and K_{disk} (Tables 4.4, 4.5, 4.6). Clearly, many tests would be required to clearly define the exact performance characteristics of a single composite. Figure 5.1 contains a stacked histogram of the friction data from Table 4.1 for all of the alternates. This plot shows that a variety of changes may be made to the baseline PM212 composite without drastically affecting frictional performance. This is realized since the histogram shows an approximate average friction coefficient of 0.3 with a range of 0.15 to 0.45. The wear results have more overlap then the friction coefficient. Without more repeat testing, it can only be said that K_{pin} for all composites at all temperatures tested primarily ranged from 10^{-6} to $10^{-5}mm^3/N\text{-}m$. This is the same for disk wear, except that its range was from -10^{-5} to $10^{-5}mm^3/N\text{-}m$ (negative sign on a wear factor indicates buildup) .

The objective of this investigation was to screen a large number of composites to obtain general trends due to compositional and processing changes. Therefore, repeat testing was not used to accurately quantify the performance of each individual composite. The rankings stated in the results pertain to the set of tests run, however they do not necessarily apply in general. Nonetheless, for screening purposes, useful information can be extracted from the results regarding composition choice. The PM212/BaF_2 composite had nearly equal performance to the baseline PM212 composite. The use of a single fluoride eliminates the time consuming process of making the eutectic fluoride. The 430NS+Ag was one of the best performing composites overall, in both friction and wear, and from low to high

temperature. The use of this composite would eliminate the need for one of the constituents (fluoride) all together.

Previous tests with plasma sprayed coatings have shown a dependency on both the silver and fluoride lubricants for lubrication over the entire temperature range (Reference 3). In those tests, a superalloy pin was slid against a disk coated with the composite. The configuration was opposite for the tests in this investigation; composite pin on superalloy disk. In the tests conducted for this investigation, oxide formation on the disk surface may have played a key role in providing lubrication at high temperature without the need of the fluoride high temperature lubricant. The oxides formed on nickel-based superalloys have been shown to have a beneficial, lubricious effect (Reference 26). In the tests performed in Reference 3, oxide formation would have been inhibited since the wear surface on the superalloy pin was in direct contact with the coated disk. Oxide formation on the superalloy disk wear track would not have been as inhibited, since the wear track was exposed to air except for the brief moment as it passed under the pin with each revolution.

In Table 4.7, some of the achieved densities were as much as 3.5% higher than theoretical. The propagated error associated with measuring the density based on obtaining dimensions and mass was less than 1%. It is likely that the additional error may have come from non-uniform powder distribution in the section used for density measurement. Small deviations from the stated composition of the powders used may also have contributed error. Thus, when a measured density is within ±3% of the theoretical, it can be considered as essentially fully dense.

The strength-porosity relationship in Figure 4.3 illustrated the importance of achieving low porosity levels to provide a composite of high strength. However friction and wear properties do not show this same strong dependence on porosity level. The exception may be at very high temperature, for the porosity level in HIPped PM212/Au may have contributed to the higher wear encountered at 900°C. Friction coefficients are slightly lower with the HIPped composites (Table 4.4). Wear factors are still in the same order of magnitude (Tables 4.5, 4.6). Hence, if the extra strength associated with full density parts is not required for a certain application, full density

processing should not be used. This is because the HIPping process used to obtain full density parts is much more labor and time intensive then the sintering process.

HIPped PM212 and PM212/Au Comparison

The pin-on-disk test results indicate that the friction and wear characteristics of the two composites were similar. In addition, both composites provided low friction and wear over the range of speeds and temperatures studied. It is also noted that the behavior of the composites in sliding against René 41 was exceptionally steady after a brief run-in period lasting less than four minutes (≈1km).

Several tests were run with PM212 at the 2.7m/s speed. It was observed that the test to test variation of the friction coefficient was typically twice as large as the variation within a single test. In several cases, the performance of the two composites were within data scatter. In general, the steady state performance of the two composites exhibited a friction coefficient of 0.3 and a wear factor in the low $10^{-5}mm^3/N\text{-}m$ range.

High friction and wear were typically encountered during a brief run-in period at the beginning of the test. This run in period typically lasted less than two minutes. Near steady state conditions were achieved in 10 minutes as shown by the run-in study for PM212/Au. The high friction and wear during run in is attributable to the high contact stresses associated with a hemisphere on flat, and the time required to develop a lubricating surface film at the contact. Previous work with PS200 coatings have also exhibited a run-in effect (Reference 15).

Typically the composite wear lowers as temperature rises from 25 to 760°C. The reduction may be from lubricious oxides formed on the superalloy (Reference 26). As temperature nears 900°C, the wear typically increases. The increase in wear at 900°C may come from the weakening of the composite with increased temperature (Reference 20). At higher temperature and higher speed PM212/Au showed higher wear than PM212. This may be due to the fact that full density was not achieved with PM212/Au, leading to notably lowered strength at higher temperatures

(Reference 20).

The tribological results for HIPped PM212 and PM212/Au were very close to results previously achieved with sintered PM212 (Reference 19). In general, sintered PM212 had friction coefficients of 0.3 to 0.4 and wear factors in the 10^{-5} to $10^{-6}mm^3/N\text{-}m$ range. The HIPped composites did encounter lower friction in some cases. Notably, neither HIPped PM212 nor HIPped PM212/Au experienced an increase in friction coefficient after 8km of sliding at 350°C that the authors of Reference 19 observed for sintered PM212.

The wear scar in Figure 3.3 was representative of typical pin surfaces after testing. There was very little difference between the wear surfaces for PM212 and PM212/Au pins. This was also true for the disk wear surfaces. This was not surprising due to the microstructural similarity of PM212 and PM212/Au. The use of EDS analyses on the SEM were selectively used in this investigation. Since the compositions of René 41, PM212 and PM212/Au contain many of the same elements, the spectra could not easily distinguish pin material from disk material and thus an accurate transfer film analysis was not possible. However, the presence of silver was detected in wear tracks from PM212 and gold in those from PM212/Au. This indicated that a transfer film was indeed developed for both composites.

It was a surprising result that a PM212/Au composite of near full density was not achieved by HIPping since it had consistently been achieved with PM212. It should be recalled that the two composites contain the same volume percentages of the three major components. The only difference is PM212 contains silver and PM212/Au contains gold as the low temperature lubricant.

The examination of the microstructures provided few, if any, answers to why full density was achieved with PM212 and not with PM212/Au. Initially, the reason was believed to be related to the higher melting point of gold. The processing temperature (1100°C) is above both the melting point of gold (1063°C) and silver (961°C). Thus, as planned, liquid phase processing of the lubricants should occur. Yet the fine web-like structure of the gold observed at high optical magnification suggested that the gold may not have completely liquified. This would have been

attributed to an error in the HIPping unit's temperature which was not the case. Yet, when the composites were examined on the SEM, the distribution of the gold and silver, as well as all other components appeared almost identical (Figure 4.7).

Finally, the structures of the gold and silver powders were examined. Since the gold particles were found to be solid, no air would have been carried into the compact inside the gold powder. A remaining possibility lies in the particle morphology difference. Figure 4.9 shows that the gold particles are spherical and the silver particles are granular. All other powders used in the composites have a granular morphology. It is possible that the spherical gold particles somehow permitted the formation of sealed air pockets in the compact during the CIPping operation which were not outgassed during the vacuum annealing and canning processes. Thus, air space could have been carried into the HIPping process which would have been trapped in the sealed can, yielding parts with porosity in the microstructure. Using gold powder with a granular morphology instead of spherical would determine if this speculation is valid. Additionally, processing the PM212/Au at a higher temperature and/or pressure might determine if the porosity was due to insufficient HIPping temperature and/or pressure.

Low Speed HIPped PM212/Au

The behavior of the composites at higher speeds in general showed a steady state behavior after a slight initial run-in period. However, at low speed with the PM212/Au, there appears to be a complicated tribological behavior. At the same conditions, the friction was as high as 0.7 ± 0.1 and as low as 0.1 ± 0.03. The run-in period is longer in time, but nearly equivalent in sliding distance to the higher speed tests. However, the use of a higher speed run-in to establish a flat on the pin accelerated the required run-in to overcome the initial high friction. The low speed tests showed a strong dependence on the formation of transfer films; both on the pin and on the disk. Most notably, when the gold film formed on the pin, the friction at 25°C was as low as 0.07.

The formation of a coherent film as found on the pin has not been observed at higher speed

tests. It is likely that at the higher speed, the rate of wear and/or heat generation is too rapid for an observable film to develop. The significant fluoride film formed at the 760°C test shown in Figure 4.12 appeared to have a negative effect on friction. The formation of too thick of a film may induce a plowing effect as the pin moves on the disk surface, causing an increased drag, and thus, higher friction. This has been observed with thick silver films previously (Reference 12).

Appendix C contains a model of the friction due to thin solid film separation of two surfaces based on the shear strength of the film as suggested by the authors of Reference 27. The model was studied to compare the low friction achieved in the cases where the gold film was formed on the pin wear surface. The minimum friction predicted by the model was 0.02. This was lower than the actual minimum achieved, which was 0.07, but within the same order of magnitude. The higher measured value may be due to an increased film shear strength due to the presence of other constituents in the film, surface roughness, and uncertainties of the real area of contact. Nonetheless, the relatively good agreement of the predicted and the measured friction coefficient indicates that surface film shear is probably playing a dominant role in friction.

CHAPTER 6

CONCLUSIONS

1. Several chromium carbide-based self-lubricating composites produced by sintering and HIPping have shown low friction and wear in sliding against a nickel-based superalloy. These composites can be used as sliding bearing and seal materials in operation from 25°C to temperatures as high as 900°C.

2. The good performance by several different composites showed that the composition of PM212 can be altered without dramatically affecting performance. This may indicate that stringent quality control on the composition itself may not be required.

3. Composites with less complex compositions than the baseline PM212 showed equivalent or better performance. Utilization of these compositions would reduce the labor and/or raw materials required.

4. Gold has been shown to be a suitable substitute for the silver in PM212. In several cases, the friction and wear of HIPped PM212 and PM212/Au were within scatter of each other. Sulfide formation that is possible with silver is not possible with gold. Thus, PM212/Au is recommended for critical applications requiring chemical stability.

5. HIPping produced full density parts of all composites except the gold containing PM212/Au. The residual porosity in PM212/Au may be caused by gas entrapment during CIPping by the spherical gold particles.

6. For the sintered composites, yield strength decreased as porosity level increased.

7. Composite wear at 25°C, 350°C, and 760°C did not show a dependence on porosity level. The exception was HIPped PM212/Au which had higher wear at 900°C than full density HIPped PM212.

8. Friction coefficients as low as 0.1±0.03 were obtained at 25°C, 0.027m/s with the PM212/Au composite, which was probably due to gold formation on the pin wear surface. This low measured friction showed good agreement with a theoretical model based on the shear strength of a gold film, indicating that film shear played a strong role in this case.

ACKNOWLEDGEMENTS

I wish to express thanks to Mr. Harold E. Sliney and Dr. Christopher DellaCorte of NASA Lewis Research Center. These two have advised and encouraged me for the past two years during my residence in the Surface Science Branch at NASA Lewis.

Thanks is also expressed to my academic advisor from Case Western Reserve University, Dr. Joseph M. Prahl. While communication has not been easy due to his training involvement as a mission specialist for the USML1 space shuttle mission, he has been a source of continued inspiration.

In addition, I wish to thank the many people at Lewis who have in many ways contributed their time and effort to this project.

Finally, I wish to express my gratitude for the financial support provided by NASA to Case Western Reserve University under cooperative agreement NCC-3-30 which made this project possible.

REFERENCES

1.) Beane, G.E. IV, Gschwender, L.J, Snyder, C.E. Jr., and Shimski, J.T., "Military Aircraft Propulsion Lubricants - Current and Future Trends," *Journal of Synthetic Lubrication*, **3**, 4, 1987.

2.) Sliney, H.E., "Solid Lubricants," NASA TM 102803, 1991.

3.) DellaCorte, C., and Sliney, H.E., "Composition Optimization of Self-Lubricating Chromium Carbide-Based Composite Coatings for Use to 760°C," *ASLE Trans*actions, **30**, 1, pp 77-83 (1987).

4.) Sliney, H.E., "Coatings for High-Temperature Bearings and Seals," NASA TM 100249, 1987.

5.) Sliney, H.E., "Some Composite Bearing and Seal Materials for Gas Turbine Applications-A Review," *ASME Transactions*, **112**, 1990.

6.) Sliney, H.E., "Composite Bearing and Seal Materials for Advanced Heat Engine Applications to 900°C," NASA TM 103612, 1990.

7.) Sliney, H.E., "Lubricating Properties of Some Bonded Fluoride and Oxide Coatings for Temperatures to 1500°F," NASA TN D-478, 1960.

8.) Sliney, H.E, "Self-Lubricating Composites of Porous Nickel and NIckel-Chromium Alloy Impregnated with Barium Fluoride-Calcium Fluoride Eutectic," ASLE Transactions, **9**, pp 336-347, 1966.

9.) Olson, K.M. and Sliney, H.E., "Additions to Fused-Fluoride Lubricant Coatings for Reduction of Low-Temperature Friction," NASA TN D-3793, 1967.

10.) Sneed, M.C., Maynard, J.L., and Brasted, R.C., *Comprehensive Inorganic Chemistry Volume II: Copper, Silver, and Gold*, D. Van Nostrand Company, Inc., New Jersey, 1954.

11.) Sliney, H.E., "Wide-Temperature-Spectrum Self-Lubricating Coatings Prepared by Plasma Spraying," NASA TM 79113, 1979.

12.) Sliney, H.E., "The Use of Silver in Self-Lubricating Coatings for Extreme Temperatures," *ASLE Transactions*, **29**, 3, pp 370-376 (1986).

13.) Wagner, R.C., and Sliney, H.E., "Effects of Silver and Group II Fluorides Addition to Plasma Sprayed Chromium Carbide High Temperature Solid Lubricant for Foil Gas Bearings to 650°C," NASA TM 86895, 1985.

14.) DellaCorte, C., and Sliney, H.E., "The Effects of Atmosphere on the Tribological Properties of a Chromium Carbide Based Coating for use to 760°C," *Lubrication Engineering*, **44**, 4, pp 338-344, (1988).

15.) DellaCorte, C., Sliney, H.E., and Deadmore, D.L., "Sputtered Silver Films to Improve Chromium Carbide Based Solid Lubricant Coatings for Use to 900°C," NASA TM-100783, *STLE Preprint* 88-AM-7F-2, 1988.

16.) Sliney, H.E., DellaCorte, C., and Deadmore, D.L., "Quality Control of the Tribological Coating-PS212," NASA TM-102067, 1989.

17.) DellaCorte, C, "Experimental Evaluation of Chromium Carbide-Based Solid Lubricant Coatings for use to 760°C," NASA CR 180808, 1987.

18.) DellaCorte, C., "Composition Optimization of Chromium Carbide-Based Coatings for Foil Gas Bearings at Temperatures to 650°C,"NASA CR 179649, 1987.

19.) DellaCorte, C., and Sliney, H.E., "Tribological Properties of PM212: A High Temperature, Self-Lubricating, Powder Metallurgy Composite," *Lubrication Engineering*, **47**, 4, pp 298-303 (1991).

20.) Edwards, P.M., Sliney, H.E., Whittenberger, J.D., Martineau, R.R., "Mechanical Strength and Thermophysical Properties of PM212: A High Temperature Self-Lubricating Powder Metallurgy Composite," NASA TM-103694, 1990.

21.) DellaCorte, C., Sliney, H.E, and Bogdanski, M.S., "Tribological and Mechanical Comparison of Sintered and HIPped PM212: High Temperature Self-Lubricating Composites," NASA TM 105379, 1992.

22.) Bogdanski, M.S., Sliney, H.E., and DellaCorte, C., "Tribological and Microstructural Comparison of PM212 and PM212/Au: Self-Lubricating, HIPped Composites," NASA TM

105615, 1992.

23.) Sliney, H.E. (U.S. Gov., NASA), U.S. Patent 4,728,488: Carbide/Fluoride/Silver Self-Lubricating Composites, March 1, 1988.

24.) Sliney, H.E. and DellaCorte, C. (U.S. Gov., NASA), U.S. Patent 5,034,187: Method of Making Carbide/Fluoride/Silver Composites,July 23, 1991.

25.) Sliney, H.E., DellaCorte, C., "A New Test Machine for Measuring Friction and Wear in Controlled Atmospheres to 1200°C," *Lubrication Engineering*, **47**, 4, pp 314-319 (1991).

26.) Sliney, H.E., Jacobson, T.P., Deadmore, D., and Miyoshi, K., "Tribology of Selected Ceramics at Temperatures to 900°C," *Ceramic Engineering and Science Proceedings*, 7, 7-8, 1986.

27.) Bowden, F.P., and Tabor, D., *The Friction and Lubrication of Solids*, Oxford University Press, 1958.

28.) Bridgman, P.W., *Studies in Large Plastic Flow and Fracture*, pp 279-292, McGraw-Hill, 1952.

APPENDIX A

PIN-ON-DISK ANALYSIS

Tribometer Sliding Distance

The pin-on-disk tribometer produces a circular wear track on the disk surface by the rotation of the disk and the stationary positioning of the pin at some radial distance from the center of the disk. The total sliding distance during a test is obtained by the following formula:

$$D_{Total} = C_{track}\,\Omega\,t$$

where:

D_{Total} = Total Sliding Distance (m)

C_{track} = wear track circumference (m/rev)

Ω = rotational speed (rev/min)

t = time (min)

Disk Wear Volume

The disk wear track is measured with a stylus profilometer, which automatically computes the area of the wear track profile. The profile area (A_{track}) is multiplied by the wear track circumference at the center of the wear track width (C_{track}) to obtain the volume of revolution which represents the disk wear volume ($V_{disk\ wear}$). See Figure 3.3 for a representative wear track profile. Thus, the following equation is used to determine the disk wear volume:

$$V_{disk\ wear} = A_{track}C_{track}.$$

Pin Wear Volume

The hemispherically tipped rider pin wear scar diameter is determined by measuring a photomicrograph of the wear scar (Figure 3.3). The wear scar diameter is then used to compute the pin wear volume through the following solid geometry equations:

$$V = \pi/6\ h\ (3a^2 + h^2) \qquad [1]$$

$$h = R - (R^2 - a^2)^{1/2} \qquad [2]$$

Substituting for h is [1] so that "a" is the only variable:

$$V = \pi/6\ [R - (R^2 - a^2)^{1/2}]\ \{3a^2 + [R-(R^2 - a^2)^{1/2}]^2\} \qquad [3]$$

Where:

V = volume of spherical tip segment worn

a = radius of the base of the spherical segment (wear scar radius)

h = height of spherical segment (axial pin motion due to pin wear)

R = hemispherical radius (pin tip radius)

Note that the wear volume increases with the cube of the wear scar diameter. Therefore, it is necessary to compute wear volume rather than wear scar diameter to determine accurate wear ratios for different tests.

Wear Factor Explanation

The wear factor (K) used in this paper is a parameter which relates the volume of material worn from a surface to the distance slid and the normal load applied at the contact. Mathematically, K is defined as:

$$K = V/(FD)$$

where:

V = volume of material worn (mm^3)

F = normal force at the sliding contact (N)

D = total sliding distance (m)

The interpretation of the numeric value for the wear factor K in the case of solid lubrication is as follows:

$K \geq 10^{-4}$ $mm^3/N\text{-}m$ High Wear

$10^{-5} \geq K \geq 10^{-6}$ mm^3/N-m	Moderate to Low Wear
$K \leq 10^{-7}$ mm^3/N-m	Very Low Wear

APPENDIX B

UNCERTAINTY ANALYSIS

Precision (External) Uncertainty

An external uncertainty analysis was not specifically performed for this set of tests on the PM200 alternates. However, previous analysis of the pin-on-disk rig has shown the following uncertainties (Reference 17):

μ external = $\pm$ 6 %

K_{pin} external = $\pm$ 12.7 %

K_{disk} external = $\pm$ 11.9 %

Several steps were taken to minimize the experimental uncertainty. A stroboscopic tachometer was used to set the disk rotational speed, thus ensuring an accurate sliding distance measurement was achieved. The magnifications used for wear scar measurement were verified with a calibration standard. Also, the relative humidity was controlled to the chamber and was monitored by as in-line probe.

Random (Internal) Uncertainty

The random uncertainty of the results were based on statistical variation within a single test and variation from test to test. Typically, a "sample" standard deviation was used to compute the variation. This was chosen instead of a "population" standard deviation since the tests represent a small part of the population of possible tests which could be performed. The test to test variation was typically twice as large as the variation within a single test.

APPENDIX C

THEORETICAL MODEL FOR SOLID-FILM LUBRICATION

A theoretical model of thin film lubrication was formulated based on that suggested by the authors of Reference 27. The specific model formulated was for a thin film of gold separating the HIPped PM212/Au pin and the René 41 disk. A flat generated by wear was assumed to exist on the tip of the pin. The real area of contact was determined as $A=W/P_s$ where W is the load and P_s is the flow pressure, approximately equal to the indentation hardness of the substrate. The frictional force was determined as $F=AS_f$ where S_f is the force required to shear the inter-atomic bonding of the film which is between the opposing surfaces. The maximum value of S_f is the shear strength of the film itself. Hence, the theoretical friction coefficient is determined as $\mu_{TH}=S_f/P_s$. The hardnesses of PM212/Au and René 41 were determined for use as the flow pressure term. The hardnesses were approximately equal, with a value of 400kg/mm^2. Transforming the hardness into units of pressure, P_s=3920MPa. The shear strength of the gold film was determined from data of shear strength versus contact pressure in Reference 28. A pin scar diameter of 2mm was used to estimate the contact pressure present between the pin and the disk. The 2mm scar diameter translates to a contact pressure of approximately 1.56MPa. The shear strength corresponding to this contact pressure from the linear regression is 62.1MPa. Using the $\mu_{TH}=S_f/P_s$ with S_f=62.1MPa and P_s=3920MPa, the theoretical friction coefficient is equal to 0.02.

APPENDIX D

COST COMPARISON OF PM212 AND PM212/Au

Cost Analysis

A cost comparison was made for the PM212 and PM212/Au composites. The comparison was based solely on material costs, and does not include processing costs. The comparison was based on typical costs of the powders in June 1991. The per gram cost, per pound cost, the cost of a small bushing (2.2cm OD, 1.3cm ID, 1.3cm thick), and the cost of cladding the ID of the same size bushing with a 1mm lining were compared. The composition of the two materials is as follows:

	430NS	Ag	Au	Eutectic
PM212	70wt%	15%	---	15%
PM212/Au	62%	---	25%	13%

The eutectic is a 62 wt% BaF_2-38 wt% CaF_2 combination. 430NS is a NiCo bonded Cr_3C_2.

The estimates presented here are based solely on material costs. Processing costs are not included. The first overview of the material costs is based on a per-pound/per-gram cost of the materials. The amounts of the components in the materials total to 1 lb for this estimate, and are stated in grams (1lb=453.6gm).

		Wt%	Amt [gm]	Cost/gm	Matl. Cost	% Cost
PM212	430NS	70.0	317.5	$0.14	$44.14	70.6
	Ag	15.0	68.0	$0.21	$13.95	22.3
	BaF_2	9.3	42.2	$0.08	$3.21	5.1
	CaF_2	5.7	25.9	$0.05	$1.24	2.0
				Total	$62.53/lb	
					$0.14/gm	

		Wt%	Amt [gm]	Cost/gm	Matl. Cost	% Cost
PM212/Au	430NS	62.0	281.2	$0.14	$39.09	2.6
	Au	25.0	113.4	$13.06	$1,481.00	97.2
	BaF_2	8.1	36.6	$0.08	$2.78	0.2
	CaF_2	4.9	22.4	$0.05	$1.08	0.1
				Total	$1,523.9/lb	
					$3.36/gm	

Based upon the comparison chart, PM212/Au costs approximately 25 times as much as the PM212 composition. To help put this into better perspective, the material cost of the small bushings are now estimated. The dimensions yield a volume of approximately 3.2cm^3. Based upon achieving the full theoretical densities of the compositions, the following summarizes the associated costs:

	Dens. [g/cm^3]	Matl. Reqd. [g]	Cost
PM212	6.6	21.1	$2.95
PM212/Au	7.5	24.0	$80.6

This estimate illustrates that the PM212/Au composition is substantially more costly than the PM212 composition. Thus, the necessity to eliminate the silver by replacement with gold must truly be merited to dictate the associated increase in cost. It should also be noted though that the costs associated with the processing of ceramics can far outweigh the material costs. However, if a 1mm lining were clad on the ID instead of making a solid busing, the volume required would be 0.6cm^3. This would translate to a cost of $0.55 for PM212 and $15.12 for PM212/Au. This would be more cost effective than making a solid bushing of PM212/Au.

This analysis can not be drawn to a general conclusion about whether the cost of materials or cost of processing would be more substantial since so many different methods of processing exist. The following are the sources for materials used in this estimate. Material costs are from the date of this estimate. The material sources for the powders used are as follows.

1.) 430NS:

Metco Corporation
1101 Prospect Avenue
Westbury, NY 11590
(516)-334-1300

2.) Ag (type DMR-3):

Degussa Corporation/Metz Division
3900 South Clinton Avenue
South Plainfield, NJ 07080
(908)-561-1100

3.) Au (mesh -100+325):

Leach & Garner Technology
P.O. Box 200
N. Attleboro, MA 02761
(508)-695-7800

4.) BaF2, CaF2:

Alfa Products

P.O. Box 8247

Ward Hill, MA 01835-0747

(800)-343-0660

Table 2.1. Rationale for compositional selections.

Composition	Selection Rationale
430NS	wear resistant matrix material, no lubricants present, what effect does this have on friction, does counterface wear increase due to lack of lubrication
430NS+Ag	PM212 without eutectic, effect of single lubricant, does performance decrease with lubricant intended for high temperature
430NS+Eut	PM212 without silver, effect of single lubricant does performance decrease with lubricant intended for low temperature
PM212	baseline dual lubricant system previously studied used as a comparison for the performance of the modified compositions
PM212/Au	PM212 with silver replaced by volumetric equivalent of gold minimizes reactivity with certain environmental contaminants, potentially raises composite operating temperature
PM212/BaF2	single fluoride (barium fluoride) in place of eutectic in PM212 can a single fluoride be used to eliminate need for making eutectic, does the higher melting point affect performance
PM212/CaF2	single fluoride (calcium fluoride) in place of eutectic in PM212 can a single fluoride be used to eliminate need for making eutectic, does the higher melting point affect performance
PM221	PM212 with approx 70% of 430NS replaced by Cr3C2, does the unbonded carbide increase the wear resistance, or does it weaken the composite and cause higher wear
PM225	PM212 with approx 30% of 430NS replaced by Cr3C2, does the unbonded carbide increase the wear resistance, or does it weaken the composite and cause higher wear
PM226	PM212 with added silver and decreased 430NS may have better low temperature performance, does increased amount of lubricant decrease wear resistance

Table 2.2. Composition of 430NS.

Element	Weight %
Chromium	48
Nickel	28
Cobalt	12
Carbon	6
Molybdenum	2
Aluminum	2
Boron	1
Silicon	1

Table 2.3. Particle size ranges and purities.

Powder	Sieve Range	Size Range [μm]	Purity
430NS	-200 + 400	37 to 74	commercial grade
chromium carbide	-200 + 400	37 to 74	commercial grade
Eutectic	-200 + 325	44 to 74	made from fluorides listed
barium fluoride	-200 + 325	44 to 74	99.9%
calcium fluoride	-200 + 325	44 to 74	99.9%
silver	-100+325	44 to 149	99.99%
gold	-100+325	44 to 149	99.9%

Table 2.4. Compositions of the alternates by weight and volume percent.

	Weight %'s of the Alternate Formulations						
Composition	430NS	Ag	Eutectic	Cr3C2	Au	BaF2	CaF2
430NS	100.0	—	—	—	—	—	—
430NS+Ag	82.0	18.0	—	—	—	—	—
430NS+Eut	82.0	—	18.0	—	—	—	—
PM212	70.0	15.0	15.0	—	—	—	—
PM212/Au	62.0	—	13.0	—	25.0	—	—
PM212/BaF2	65.3	13.9	—	—	—	20.8	—
PM212/CaF2	70.0	15.0	—	—	—	—	15.0
PM221	18.2	15.0	15.0	51.8	—	—	—
PM225	40.0	15.0	15.0	30.0	—	—	—
PM226	59.5	25.8	14.7	—	—	—	—
	Volume %'s of the Alternate Formulations						
Composition	430NS	Ag	Eutectic	Cr3C2	Au	BaF2	CaF2
430NS	100.0	—	—	—	—	—	—
430NS+Ag	87.2	12.8	—	—	—	—	—
430NS+Eut	72.6	—	27.4	—	—	—	—
PM212	66.2	9.4	24.4	—	—	—	—
PM212/Au	66.4	—	24.0	—	9.7	—	—
PM212/BaF2	62.6	8.9	—	—	—	28.5	—
PM212/CaF2	62.0	8.8	—	—	—	—	29.2
PM221	16.8	9.2	23.9	50.1	—	—	—
PM225	37.3	9.3	24.1	29.3	—	—	—
PM226	58.3	16.8	24.8	—	—	—	—

Table 2.5. Composition of René 41.

Element	Weight %
Nickel	Balance
Chromium	19.00
Molybdenum	10.00
Cobalt	10.00
Titanium	3.00
Aluminum	1.50
Iron	1.00
Carbon	0.10
Silicon	0.10
Manganese	0.05
Sulphur	0.01
Boron	0.005

Table 3.1 Tribological test conditions for PM212 and PM212/Au comparison.

Sliding Velocity [m/s]	Composite	Temperature [°C]	Tests Performed
10	PM212	25	1@70min
	"	350	"
	"	760	"
	PM212/Au	25	"
	"	350	"
	"	760	"
2.7	PM212	25	4@60min, 2@70min
	"	350	"
	"	760	4@30min, 2@70min
	"	900	4@60min, 1@70min
	PM212/Au	25	2@70min,2@1min,2@10min
	"	350	2@70min
	"	760	"
	"	900	"
0.27	PM212	25	1@70min
	"	350	"
	"	760	"
	"	900	"
	PM212/Au	25	"
	"	350	"
	"	760	"
	"	900	"

Table 4.1 Friction coefficient screening summary for sintered and HIPped alternates at 2.7m/s.

Sintered Composition	Temperature		
	25°C	350°C	760°C
PM212	0.34±0.02 (a)	0.44±0.09	0.35±0.03
PM212/BaF2	0.37±0.04	0.39±0.07	0.27±0.03
PM212/CaF2	0.38±0.03	0.43±0.05	0.23±0.02
PM221	0.44±0.07	0.39±0.05	0.27±0.02
PM225	0.44±0.05	0.42±0.03	0.24±0.02
PM226	0.31±0.01	0.37±0.03	0.26±0.03

HIPped Composition	Temperature			
	25°C	350°C	760°C	900°C
430NS	0.36±0.05	0.42±0.04	0.23±0.02	0.23±0.01
430NS+Ag	0.32±0.05	0.28±0.03	0.16±0.05	0.22±0.01
430NS+Eut	0.38±0.02	0.30±0.02	0.28±0.02	0.29±0.01
PM212	0.40±0.06	0.26±0.06	0.28±0.02	0.25±0.01
PM212/Au	0.33±0.03	0.24±0.01	0.29±0.02	0.33±0.01
PM212/BaF2	0.33±0.02	0.27±0.01	0.29±0.03	0.31±0.02
PM212/CaF2	0.30±0.02	0.27±0.02	0.31±0.03	0.42±0.05
PM221	0.36±0.04	0.29±0.04	0.28±0.04	0.26±0.03
PM225	0.32±0.05	0.25±0.04	0.27±0.01	0.23±0.02
PM226	0.29±0.02	0.34±0.01	0.21±0.03	0.25±0.02

(a) Variation is ± 1 standard deviation measured during testing.
One specimen set of each composite was tested at each temperature.

Table 4.2 Pin wear [mm^3/N-m] screening summary for sintered and HIPped alternates at 2.7m/s

Sintered Composition	Temperature			
	25 °C	350 °C	760 °C	
PM212	[a]2.5×10^{-5}	1.8×10^{-5}	6.0×10^{-6}	
PM212/BaF2	3.3×10^{-5}	2.0×10^{-5}	3.3×10^{-5}	
PM212/CaF2	5.1×10^{-5}	5.1×10^{-5}	1.2×10^{-6}	
PM221	1.7×10^{-4}	5.1×10^{-5}	1.5×10^{-6}	
PM225	9.2×10^{-5}	6.8×10^{-5}	2.0×10^{-6}	
PM226	2.4×10^{-5}	2.5×10^{-5}	1.7×10^{-6}	
HIPped Composition	Temperature			
	25 °C	350 °C	760 °C	900 °C
430NS	1.8×10^{-6}	1.6×10^{-5}	8.1×10^{-7}	5.1×10^{-7}
430NS+Ag	2.0×10^{-5}	1.6×10^{-5}	1.8×10^{-6}	3.9×10^{-7}
430NS+Eut	1.3×10^{-5}	1.8×10^{-5}	1.5×10^{-6}	3.0×10^{-6}
PM212	2.3×10^{-5}	2.9×10^{-5}	5.7×10^{-7}	1.2×10^{-6}
PM212/Au	1.6×10^{-6}	2.3×10^{-5}	3.6×10^{-6}	6.2×10^{-5}
PM212/BaF2	2.2×10^{-6}	2.6×10^{-5}	5.7×10^{-7}	1.3×10^{-5}
PM212/CaF2	3.0×10^{-5}	2.6×10^{-5}	2.5×10^{-5}	2.0×10^{-5}
PM221	4.1×10^{-6}	3.2×10^{-5}	1.2×10^{-6}	1.7×10^{-6}
PM225	2.7×10^{-5}	2.6×10^{-5}	7.3×10^{-7}	2.0×10^{-6}
PM226	1.9×10^{-5}	2.7×10^{-5}	2.0×10^{-6}	2.0×10^{-6}

[a]One specimen set of each composite was tested at each temperature.

Table 4.3 Disk wear [mm^3/N-m] screening summary for sintered and HIPped alternates at 2.7m/s

Sintered Composition	Temperature			
	25 °C	350 °C	760 °C	
PM212	[b]6.4×10^{-7}	3.5×10^{-6}	[a]-2.9×10^{-5}	
PM212/BaF2	6.8×10^{-6}	4.0×10^{-6}	-2.2×10^{-5}	
PM212/CaF2	5.3×10^{-6}	3.4×10^{-6}	4.7×10^{-6}	
PM221	6.7×10^{-5}	1.3×10^{-5}	4.3×10^{-6}	
PM225	3.7×10^{-5}	1.1×10^{-5}	9.8×10^{-7}	
PM226	6.8×10^{-6}	1.0×10^{-5}	8.3×10^{-6}	
HIPped Composition	Temperature			
	25 °C	350 °C	760 °C	900 °C
430NS	4.1×10^{-5}	6.7×10^{-5}	5.0×10^{-5}	4.2×10^{-5}
430NS+Ag	1.8×10^{-5}	6.0×10^{-6}	2.5×10^{-5}	2.0×10^{-5}
430NS+Eut	1.9×10^{-5}	1.9×10^{-6}	1.6×10^{-5}	-3.7×10^{-6}
PM212	4.7×10^{-5}	1.4×10^{-5}	1.8×10^{-5}	-8.7×10^{-7}
PM212/Au	5.7×10^{-5}	-5.0×10^{-6}	3.3×10^{-6}	-2.5×10^{-5}
PM212/BaF2	1.7×10^{-5}	-2.5×10^{-7}	5.6×10^{-6}	-1.8×10^{-6}
PM212/CaF2	9.7×10^{-6}	-3.0×10^{-6}	-9.6×10^{-6}	-1.5×10^{-5}
PM221	6.5×10^{-5}	2.0×10^{-5}	4.5×10^{-6}	1.4×10^{-7}
PM225	1.2×10^{-5}	4.9×10^{-6}	1.1×10^{-5}	2.5×10^{-6}
PM226	9.7×10^{-6}	6.7×10^{-6}	1.7×10^{-5}	-6.0×10^{-7}

[a]Negative number indicates buildup occurred on disk.
[b]One specimen set of each composite was tested at each temperature.

Table 4.4 Friction coefficient rankings for sintered and HIPped alternates at 2.7 m/s

Rank	Sintered Composite	Average Friction Coefficient Over Temperature Range
1	PM226	[a]0.31±0.06
2	PM212/BaF2	0.34±0.06
3	PM212/CaF2	0.34±0.10
4	PM221	0.37±0.09
5	PM225	0.37±0.11
6	PM212	0.38±0.06
Rank	**HIPped Composite**	**Average Friction Coefficient Over Temperature Range**
1	430NS+Ag	0.25±0.07
2	PM225	0.27±0.04
3	PM226	0.27±0.06
4	PM221	0.30±0.04
5	PM212/Au	0.30±0.04
6	PM212	0.30±0.07
7	PM212/BaF2	0.30±0.03
8	430NS	0.31±0.10
9	430NS+Eut	0.31±0.05
10	PM212/CaF2	0.33±0.07

[a]One standard deviation about average friction coefficient over temperature range.

Table 4.5 Pin wear rankings for sintered and HIPped alternates at 2.7 m/s

Rank	Sintered Composite	Average Pin Wear Over Temperature Range	Range of Wear Factor
1	PM226	1.7×10^{-5}	1.7×10^{-6} to 2.5×10^{-5}
2	PM212/BaF2	2.9×10^{-5}	2.0×10^{-5} to 3.3×10^{-5}
3	PM212	3.4×10^{-5}	1.8×10^{-5} to 6.0×10^{-5}
4	PM212/CaF2	3.4×10^{-5}	1.2×10^{-6} to 5.1×10^{-5}
5	PM225	5.4×10^{-5}	2.0×10^{-6} to 9.2×10^{-5}
6	PM221	7.4×10^{-5}	1.5×10^{-6} to 1.7×10^{-4}
Rank	**HIPped Composition**	**Average Pin Wear Over Temperature Range**	**Range of Wear Factor**
1	430NS	8.8×10^{-6}	5.1×10^{-7} to 1.8×10^{-5}
2	430NS+Eut	8.9×10^{-6}	1.5×10^{-6} to 1.8×10^{-5}
3	430NS+Ag	9.5×10^{-6}	3.9×10^{-7} to 2.0×10^{-5}
4	PM226	1.3×10^{-5}	2.0×10^{-6} to 2.7×10^{-5}
5	PM212	1.3×10^{-5}	5.7×10^{-7} to 2.9×10^{-5}
6	PM225	1.4×10^{-5}	7.3×10^{-7} to 2.6×10^{-5}
7	PM212/BaF2	1.5×10^{-5}	5.7×10^{-7} to 2.6×10^{-5}
8	PM221	1.9×10^{-5}	1.2×10^{-6} to 4.1×10^{-5}
9	PM212/CaF2	2.5×10^{-5}	2.0×10^{-5} to 3.0×10^{-5}
10	PM212/Au	2.6×10^{-5}	3.6×10^{-6} to 6.2×10^{-5}

Table 4.6 Disk wear rankings for sintered and HIPped alternates at 2.7 m/s

Rank	Sintered Composite	Average Disk Wear Over Temperature Range	Range of Wear Factor
1	PM212	2.1×10^{-6}	-2.9×10^{-5} to 3.5×10^{-6}
2	PM212/CaF2	4.5×10^{-6}	3.4×10^{-6} to 5.3×10^{-6}
3	PM212/BaF2	5.4×10^{-6}	-2.2×10^{-5} to 6.8×10^{-6}
4	PM226	8.4×10^{-6}	6.8×10^{-6} to 1.0×10^{-5}
5	PM225	1.6×10^{-5}	9.8×10^{-7} to 3.7×10^{-5}
6	PM221	2.8×10^{-5}	4.3×10^{-6} to 6.7×10^{-5}
Rank	**HIPped Composition**	**Average Disk Wear Over Temperature Range**	**Range of Wear Factor**
1	PM212/CaF2	[a]-4.5×10^{-6}	-1.5×10^{-5} to 9.7×10^{-6}
2	PM212/BaF2	5.1×10^{-6}	-1.8×10^{-6} to 1.7×10^{-5}
3	PM212/Au	7.6×10^{-6}	-2.5×10^{-5} to 5.7×10^{-5}
4	PM225	7.6×10^{-6}	2.5×10^{-6} to 1.2×10^{-5}
5	PM226	8.2×10^{-6}	-6.0×10^{-7} to 1.7×10^{-5}
6	430NS+Eut	8.3×10^{-6}	-3.7×10^{-6} to 1.9×10^{-5}
7	430NS+Ag	1.7×10^{-5}	6.0×10^{-6} to 2.5×10^{-5}
8	PM212	2.0×10^{-5}	-8.7×10^{-7} to 4.7×10^{-5}
9	PM221	2.2×10^{-5}	1.4×10^{-7} to 6.5×10^{-5}
10	430NS	5.0×10^{-5}	4.1×10^{-5} to 6.7×10^{-5}

[a]Negative number indicates buildup occurred on disk.

Table 4.7 Density results from sintering and HIPping for the alternates.

Composition (Sintered)	Theoretical Density [g/cm^3]	Measured Density [g/cm^3]	% of Theoretical Achieved	% Residual Porosity
430NS	6.99	3.70	52.9	47.1
PM212	6.61	5.20	78.6	21.4
PM212/BaF2	6.70	5.36	80.0	20.0
PM212/CaF2	6.19	4.18	67.6	32.4
PM221	6.46	4.25	65.7	34.3
PM225	6.52	4.26	65.4	34.6
PM226	6.85	5.60	81.8	18.2
Composition (HIPped)	Theoretical Density [g/cm^3]	Measured Density [g/cm^3]	% of Theoretical Achieved (a)	% Residual Porosity (b)
430NS	6.99	7.23	103.5	-3.5
430NS + Ag	7.44	7.58	101.9	-1.9
430NS + Eut.	6.19	6.32	102.1	-2.1
PM212	6.61	6.70	101.4	-1.4
PM212/Au	7.48	6.34	84.8	15.2
PM212/BaF2	6.70	6.76	100.9	-0.9
PM212/CaF2	6.19	6.25	101.0	-1.0
PM221	6.46	6.32	97.8	2.2
PM225	6.52	6.53	100.1	-0.1
PM226	6.85	6.94	101.3	-1.3
PM221 (45ksi)	6.46	6.41	99.3	0.7
PM225 (45ksi)	6.52	6.55	100.4	-0.4

(a) Values over 100% are indicative of experimental error
(b) Negative values are indicative of experimental error

Table 4.8 0.2% Compressive yield strength [MPa] of the sintered alternates.

	Temperature			
Composition	25°C	350°C	760°C	900°C
PM212	346.1	333.7	95.1	20.0
PM212/BaF2	268.9	246.8	82.7	9.7
PM212/CaF2	78.6	62.7	49.6	24.1
PM221	120.0	101.4	77.9	26.2
PM225	86.9	80.0	66.9	27.6
PM226	348.2	269.6	108.9	30.3

Table 4.9 Tribological data summary for HIPped PM212 and PM212/Au comparison

Sliding Velocity, m/sec	Composite	Temperature, °C	Friction[a] Coefficient	Test-to-Test Variation	Single Test Variation, s(μ)	K_{pin}[b], $mm^3/N\text{-}m$	K_{disk}[c], $mm^3/N\text{-}m$
10	PM212	25	0.23	----	0.02	1.2×10^{-5}	1.9×10^{-6}
	PM212	350	.36	----	.04	2.8×10^{-5}	-2.0×10^{-7}
	PM212	760	.25	----	.04	1.7×10^{-5}	2.9×10^{-6}
	PM212/Au	25	.27	----	.04	1.4×10^{-5}	7.6×10^{-7}
	PM212/Au	350	.25	----	.04	2.0×10^{-5}	6.3×10^{-7}
	PM212/Au	760	.36	----	.02	7.6×10^{-5}	5.7×10^{-6}
2.7	PM212	25	0.37	0.04	0.02	$1.8\pm0.5\times10^{-5}$	$1.2\pm1.7\times10^{-5}$
	↓	350	.34	.08	.03	$2.5\pm0.3\times10^{-5}$	$4.2\pm0.6\times10^{-5}$
		760	.32	.04	.02	[d]5×10^{-6}	$1.2\pm1.7\times10^{-5}$
		900	.28	.04	.01	$5.4\pm3.0\times10^{-6}$	$-3.8\pm5.5\times10^{-6}$
	PM212/Au	25	.36	----	.03	1.9×10^{-5}	5.9×10^{-6}
	↓	350	.27	----	.02	2.6×10^{-5}	-3.3×10^{-6}
		760	.35	----	.04	1.2×10^{-5}	-1.5×10^{-6}
		900	.32	----	.01	4.3×10^{-5}	-1.9×10^{-5}
0.27	PM212	25	0.51	----	0.04	4.5×10^{-5}	4.6×10^{-4}
	↓	350	.40	----	.03	2.0×10^{-5}	8.8×10^{-6}
		760	.23	----	.06	1.9×10^{-6}	1.1×10^{-4}
	PM212/Au	900	.26	----	.01	2.4×10^{-5}	-5.9×10^{-5}
		25	.30	----	.03	2.4×10^{-5}	1.1×10^{-4}
	↓	350	.36	----	.04	4.5×10^{-5}	-3.1×10^{-6}
		760	.28	----	.02	7.7×10^{-7}	9.2×10^{-6}
		900	.28	----	.02	3.8×10^{-5}	-4.6×10^{-5}

[a]Overall average for 2.7 m/sec tests, single test average for others.
[b]K average for 2.7 m/sec tests with PM212, s(K) as uncertainty.
[c]Negative sign indicates material buildup during test.
[d]For this condition, range was 0.05×10^{-5} to 1.7×10^{-5}.

Table 4.10 Results from low speed (0.027 m/s) tests of PM212/Au

Elevated Speed run-in	Time at 0.027 m/s	Temperature, °C	Sliding Distance, m at 0.207 m/s	Friction Coefficient and Variation,[a]	K pin, $mm^3/N\text{-}m$	K disk, $mm^3/N\text{-}m$
none	70 min	25	113	0.70±0.1	7.6×10^{-6}	7.6×10^{-5}
none	70 min	350	113	0.39±0.09	4.7×10^{-5}	-3.2×10^{-5}
none	70 min	760	113	0.48±0.08	9.5×10^{-5}	-3.8×10^{-4}
70 min, 0.95 m/s	70 min	25	113	0.25±0.08	3.3×10^{-5}	4.3×10^{-5}
70 min, 0.95 m/s	70 min	760	113	0.27±0.07	9.1×10^{-5}	-2.4×10^{-5}
none	15.4 hr	25	1497	0.70±0.1	6.6×10^{-5}	3.0×10^{-3}
none	88.0 hr	25	8554	0.10±0.03	2.6×10^{-6}	1.5×10^{-5}
10 min, 2.7 m/s	2 hr/	25 to 800		0.25±0.50		
	66.0 hr	25	6610	0.10±0.03	3.0×10^{-6}	-9.7×10^{-6}
20 min, 2.7 m/s	4 hr	25	389	0.34±0.11	3.2×10^{-5}	-3.7×10^{-5}
20 min, 2.7 m/s	4 hr	350	389	0.26±0.04	3.6×10^{-5}	-6.7×10^{-5}
20 min, 2.7 m/s	4 hr	760	389	0.41±0.03	2.2×10^{-4}	-8.9×10^{-5}

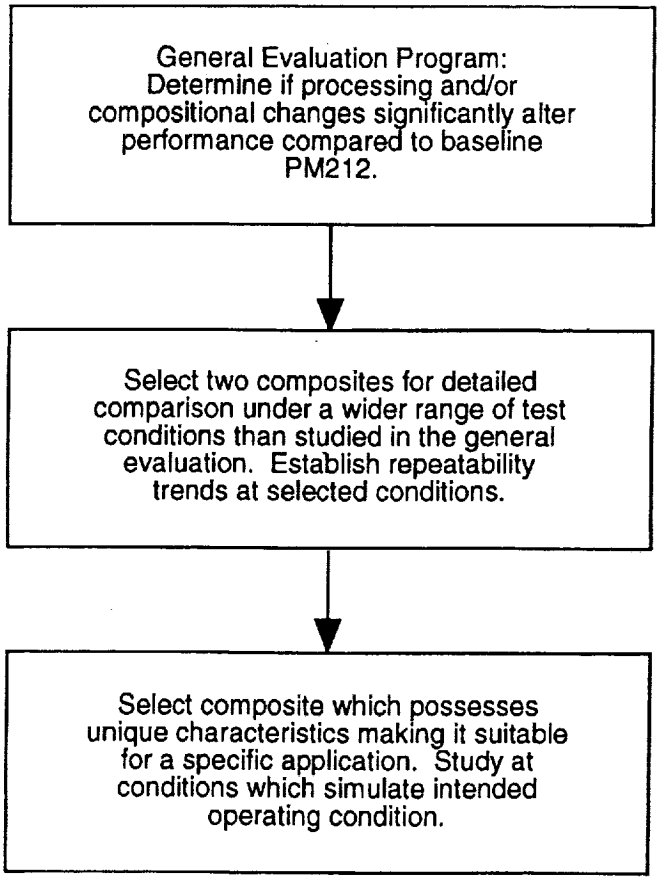

Figure 1.1.—Approach utilized for this investigation.

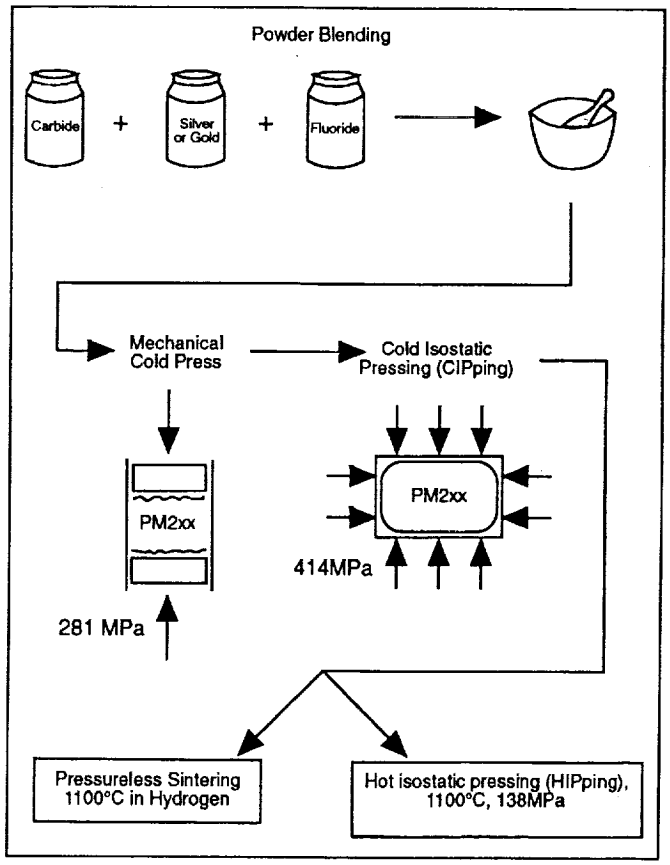

Figure 2.1.—Powder metallurgy (PM) processing routes to make composites.

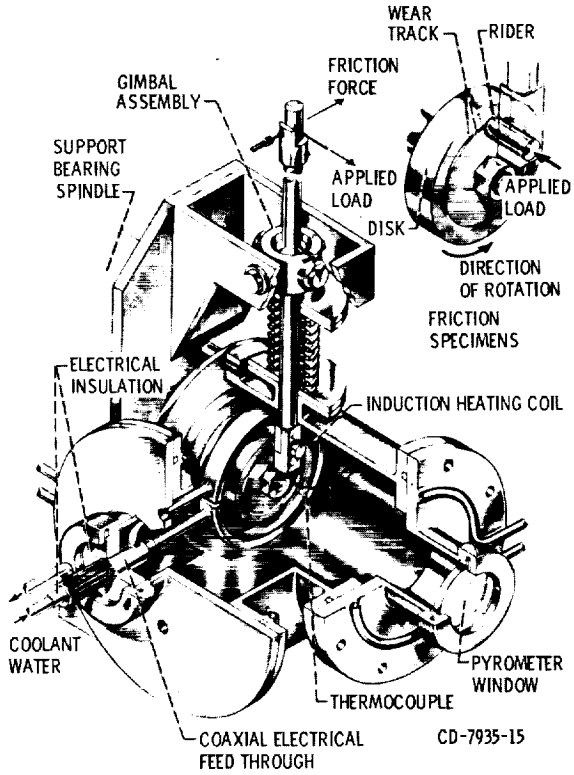

Figure 3.1.—Induction heated pin-on-disk rig.

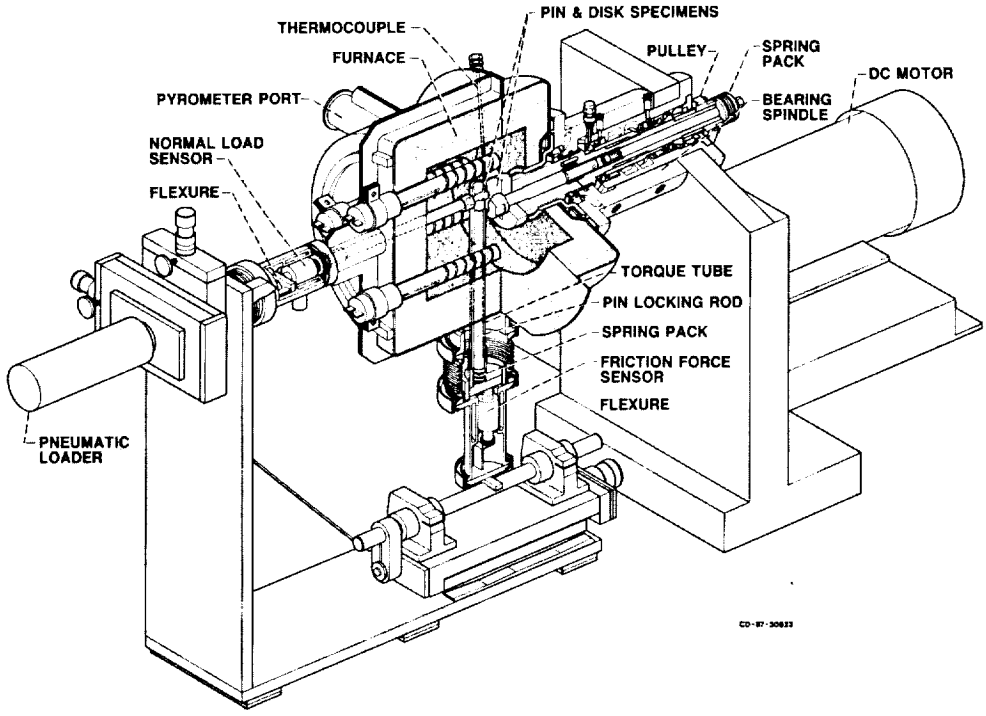

Figure 3.2.—Furnace heated pin-on-disk rig.

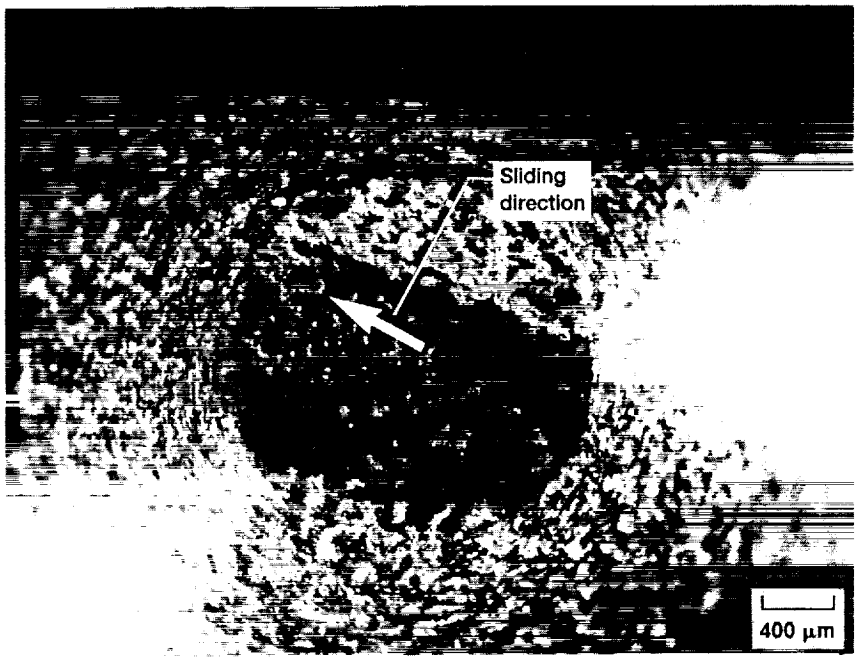

(a) Pin wear scar.

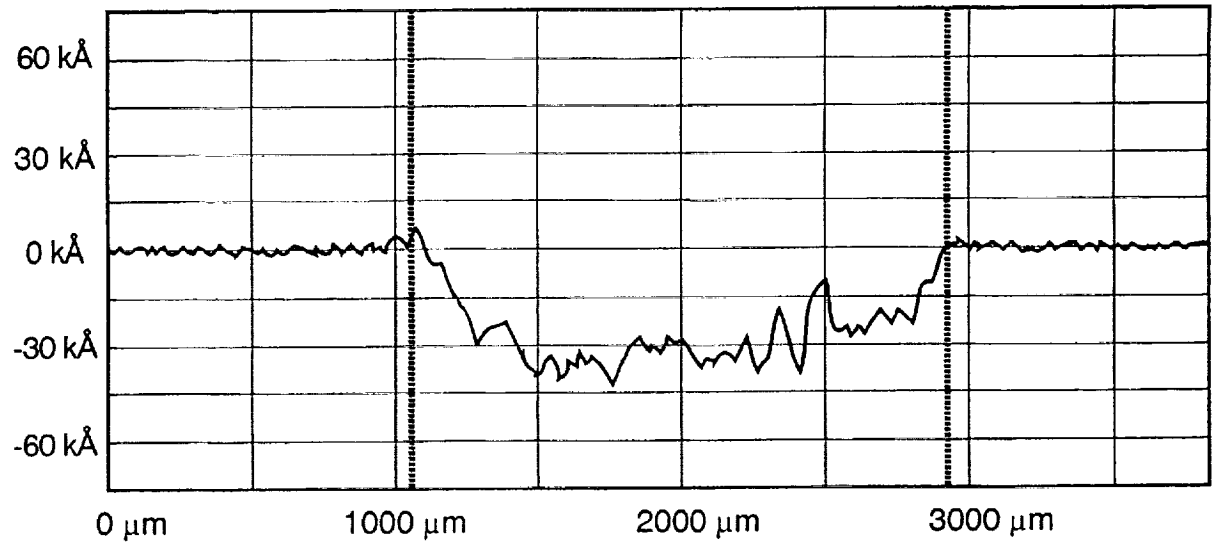

(b) Disk wear track profile.

Figure 3.3.—Wear measurements of pin and disk specimens.

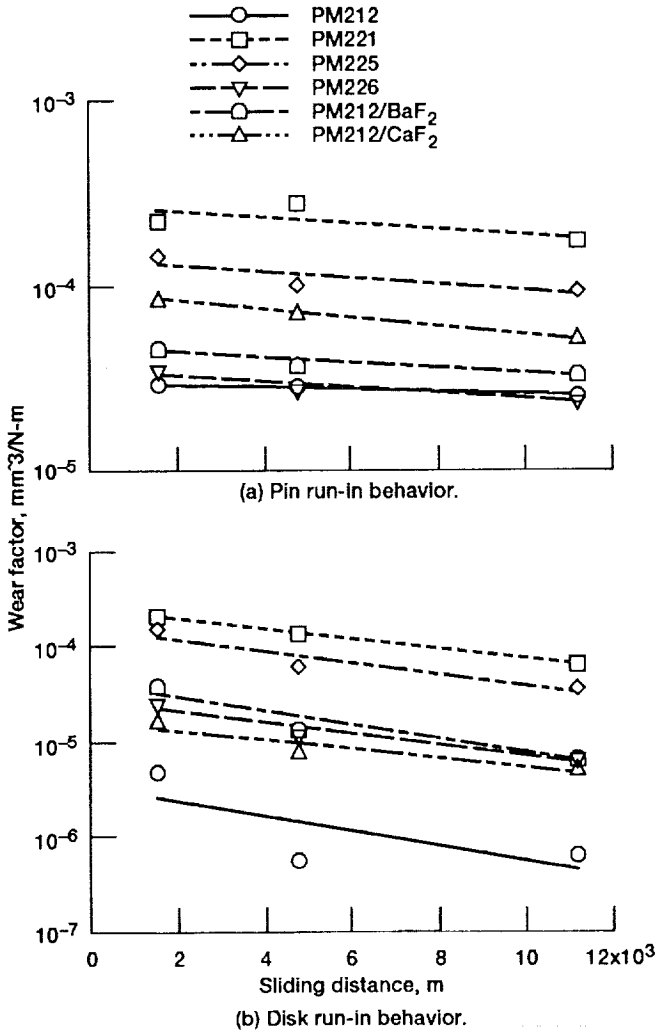

Figure 4.1.—Run-in behavior of the sintered alternates at 25 °C.

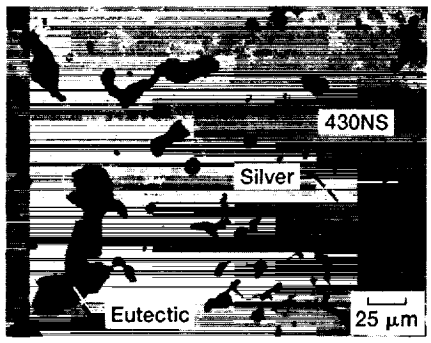

(a) PM212 (HIPped).

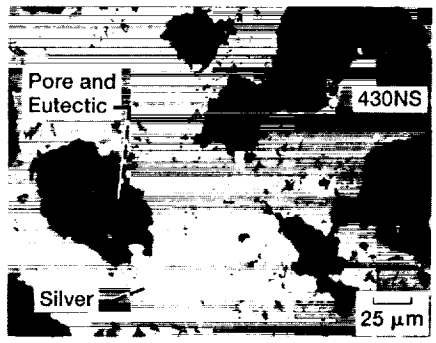

(b) PM212 (sintered).

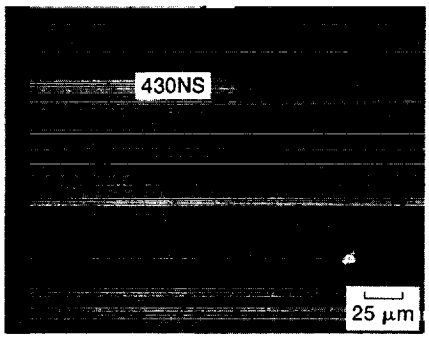

(c) 430NS (HIPped).

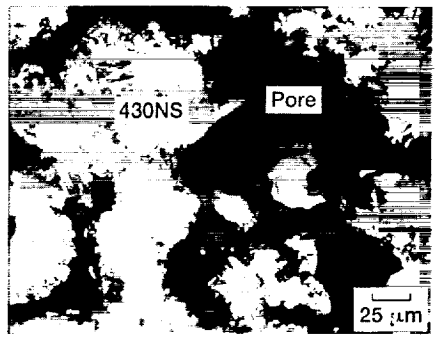

(d) 430NS (sintered).

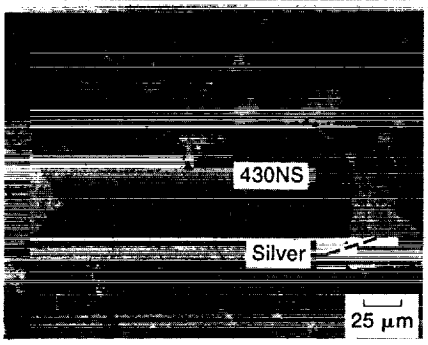

(e) 430NS + Ag (HIPped).

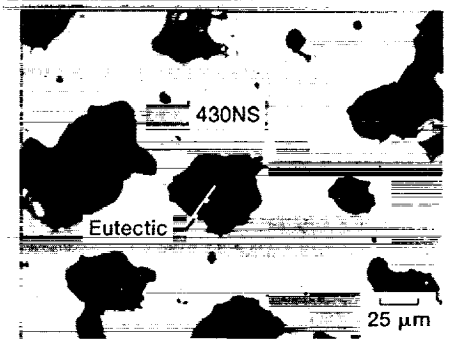

(f) 430NS + Eut (HIPped).

Figure 4.2.—Optical micrographs of the composite microstructures.

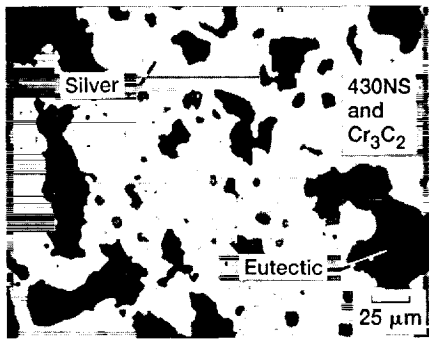

(a) PM221 (HIPped).

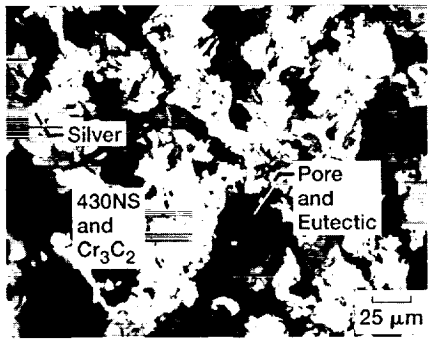

(b) PM221 (sintered).

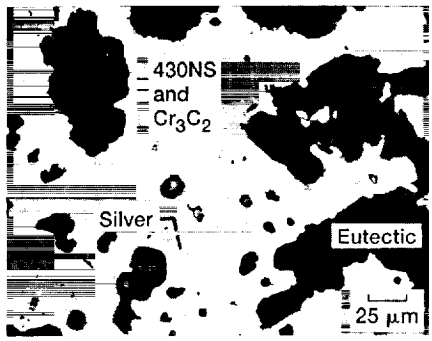

(c) PM225 (HIPped).

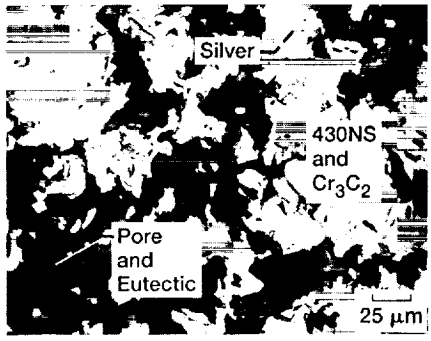

(d) PM225 (sintered).

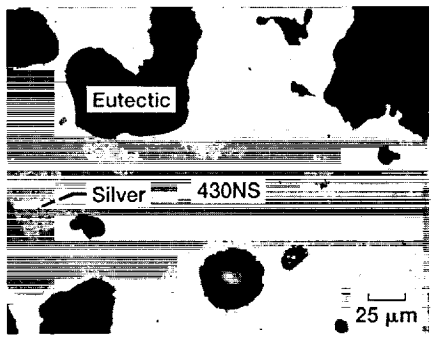

(e) 430NS + Ag (HIPped).

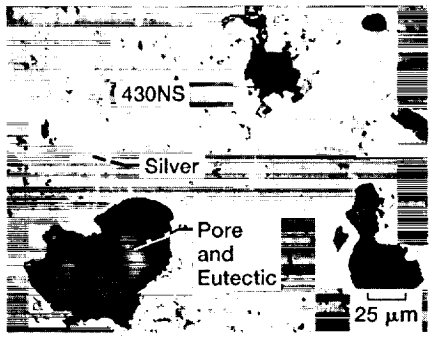

(f) 430NS + Eut (HIPped).

Figure 4.2.—Continued.

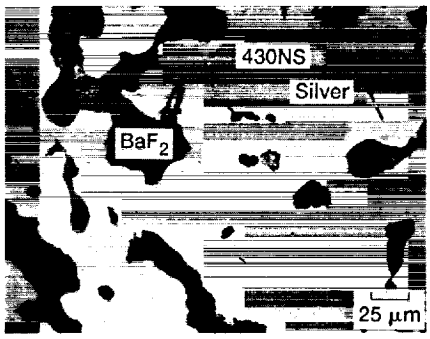

(a) PM212/BaF_2 (HIPped).

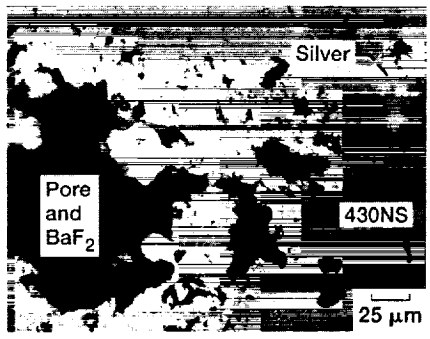

(b) PM212/BaF_2 (sintered).

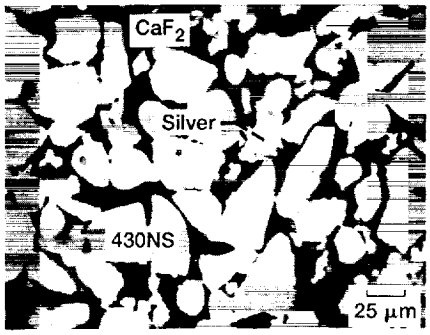

(c) PM212/CaF_2 (HIPped).

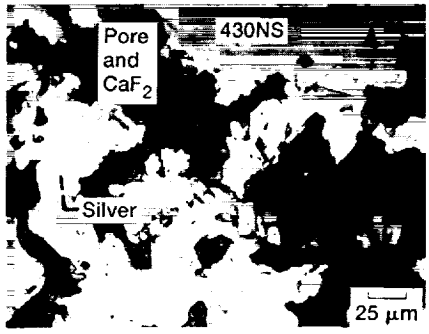

(d) PM212/CaF_2 (sintered).

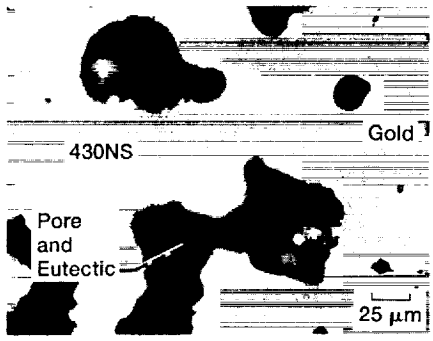

(e) PM212/Au (HIPped).

Figure 4.2.—Concluded.

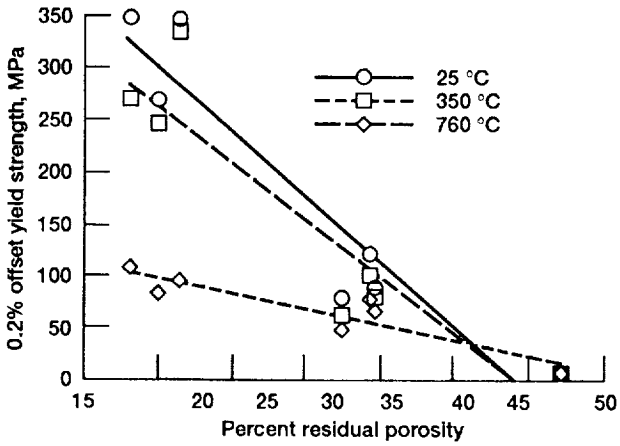

Figure 4.3.—Yield strength versus percent residual porosity in the sintered alternates.

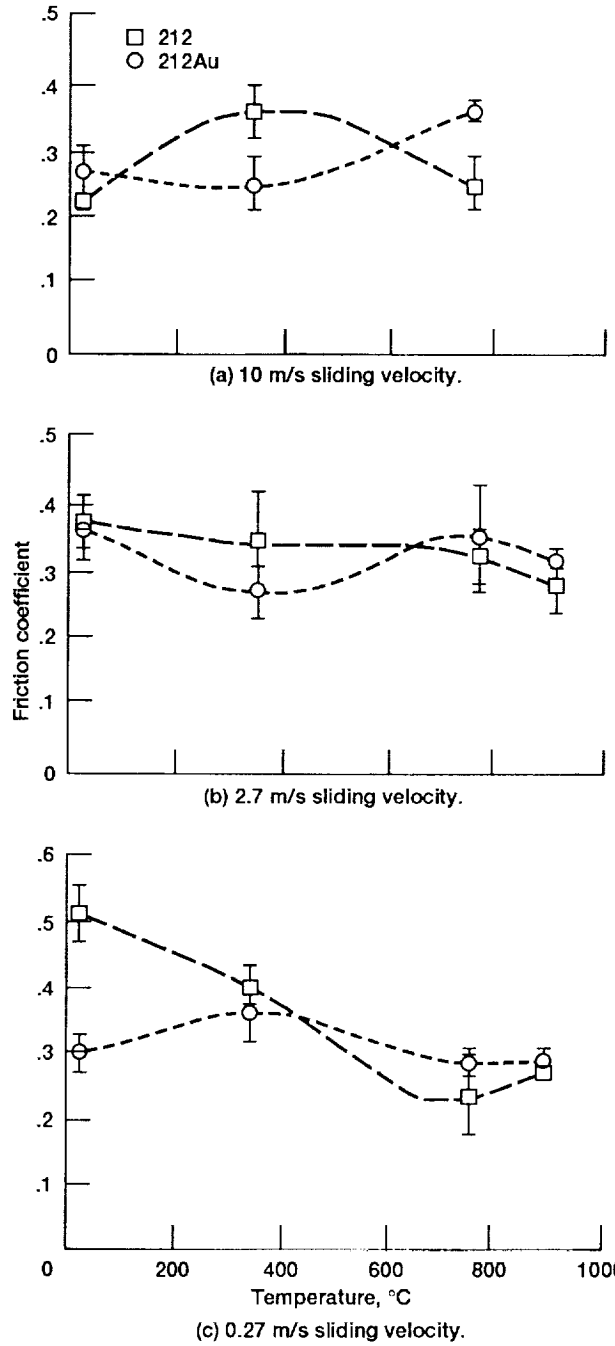

Figure 4.4.—Friction coefficient versus temperature for HIPped PM212 and PM212/Au.

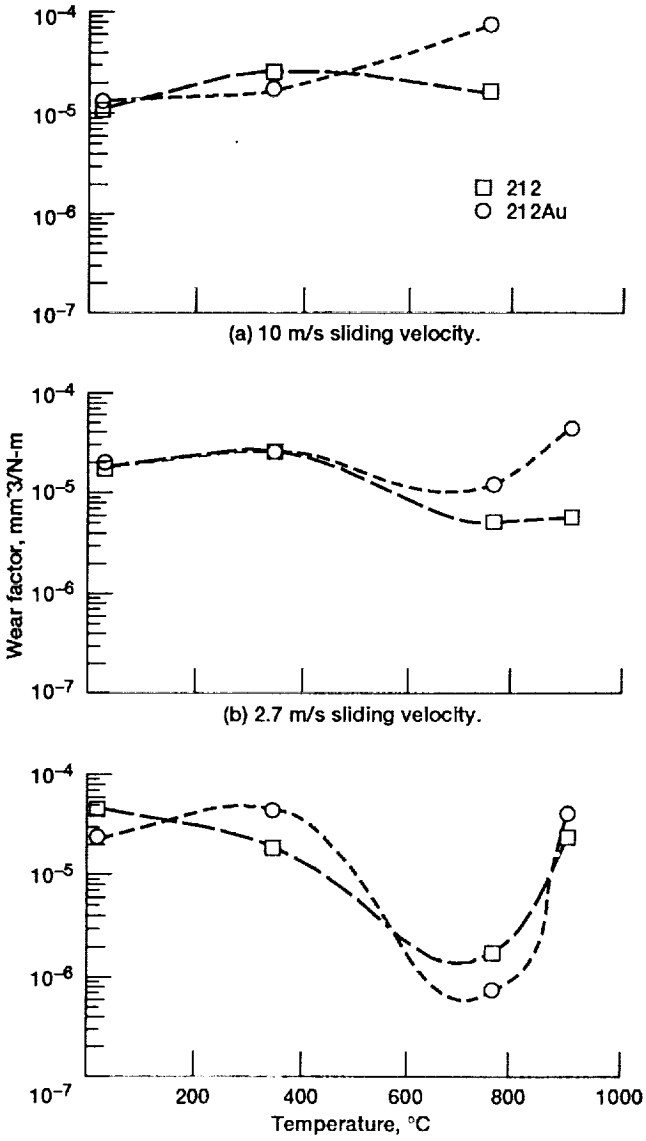

Figure 4.5.—Pin wear factor versus temperature for HIPped PM212 and PM212/Au.

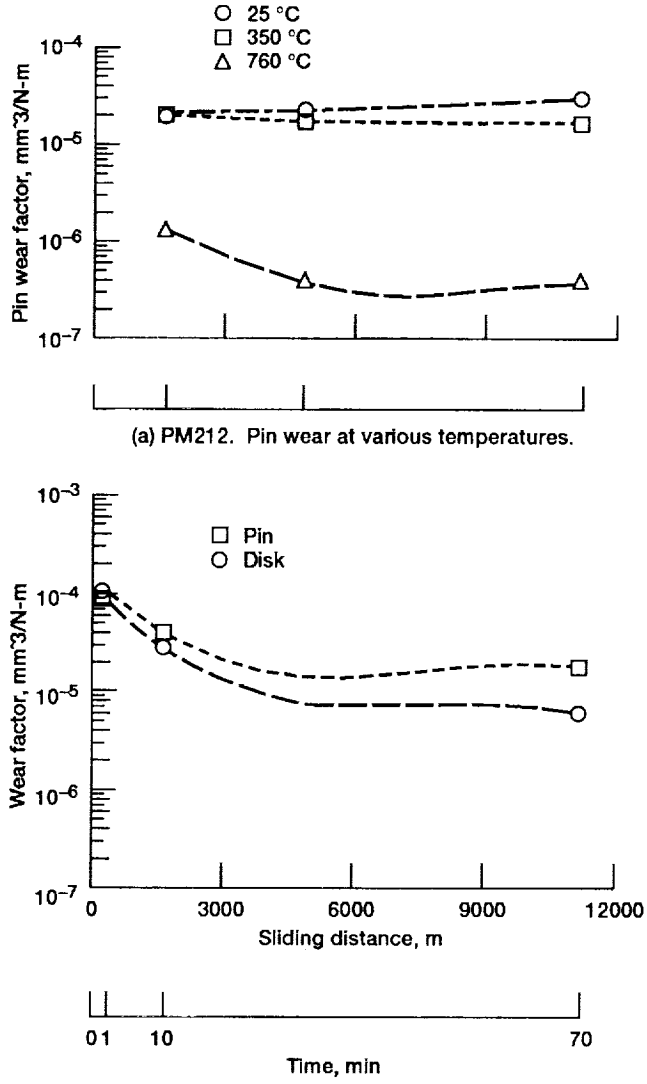

Figure 4.6.—Run-in effects on wear of HIPped PM212 and PM212/Au.

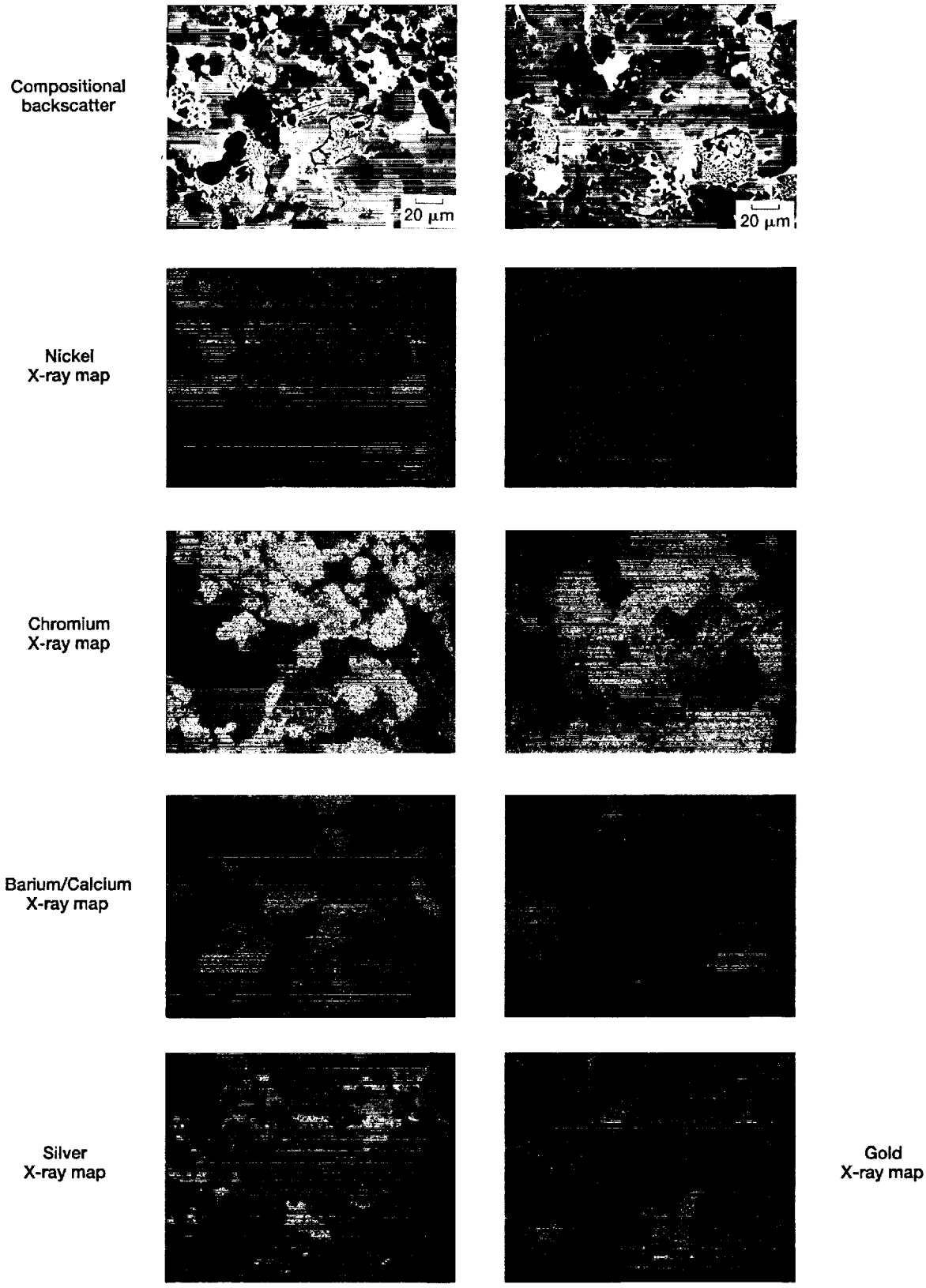

(a) PM212 (b) PM212/Au

Figure 4.7.—SEM images showing elemental distribution for HIPped PM212 and PM212/Au.

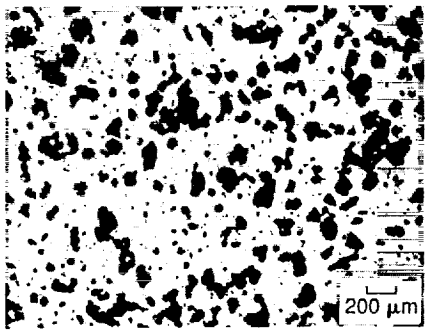

(a) PM212 (optical).

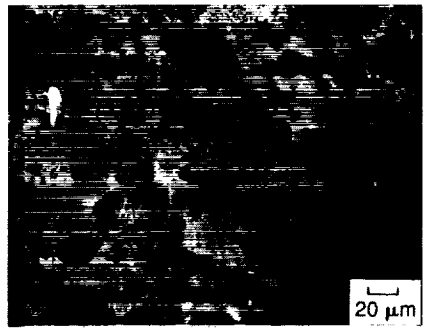

(b) PM212 (SEM).

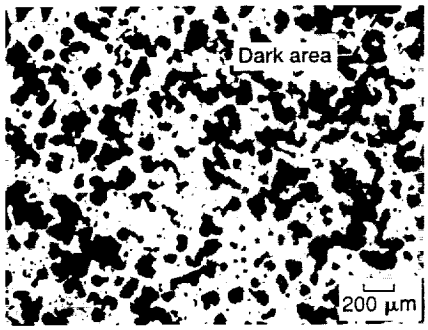

(c) PM212 (optical).

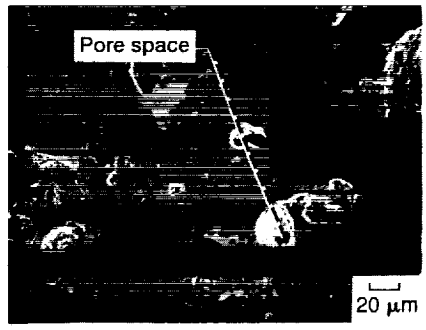

(d) PM212 (SEM).

Figure 4.8.—Low magnification optical micrographs and high magnification SEM micrographs of HIPped PM212 and PM212/Au.

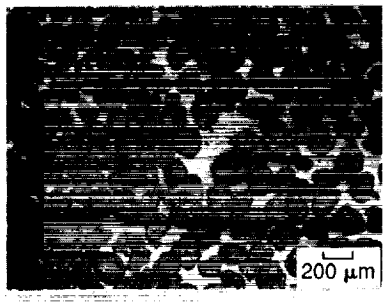

(a) Silver particles.

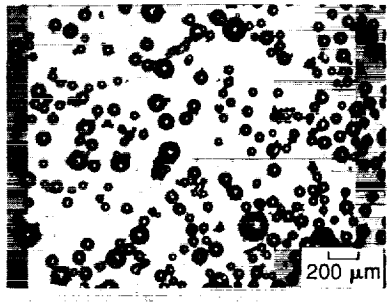

(b) Gold particles.

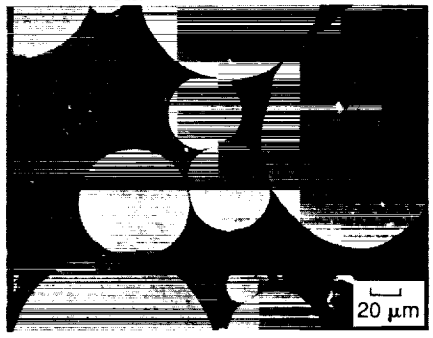

(c) Cross section of gold powder (SEM).

Figure 4.9.—Gold and silver powder morphology.

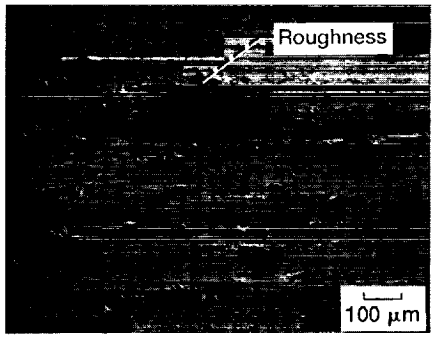

(a) 25 °C, no run-in.

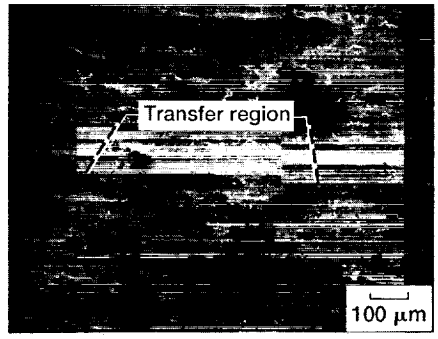

(b) 25 °C, 0.95 m/s run-in.

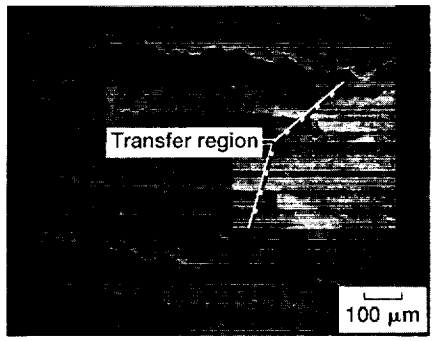

(c) 350 °C, no-run-in.

Figure 4.10.—SEM micrographs of wear tracks from 0.027 m/s tests of HIPped PM212/Au (25 °C and 350 °C).

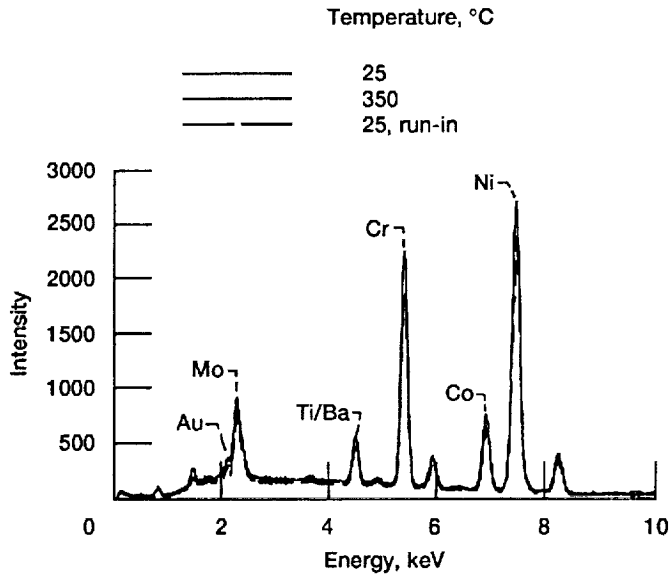

Figure 4.11.—EDS spectra of wear tracks from 0.027m/s tests of HIPped PM212/Au (25 °C and 350 °C).

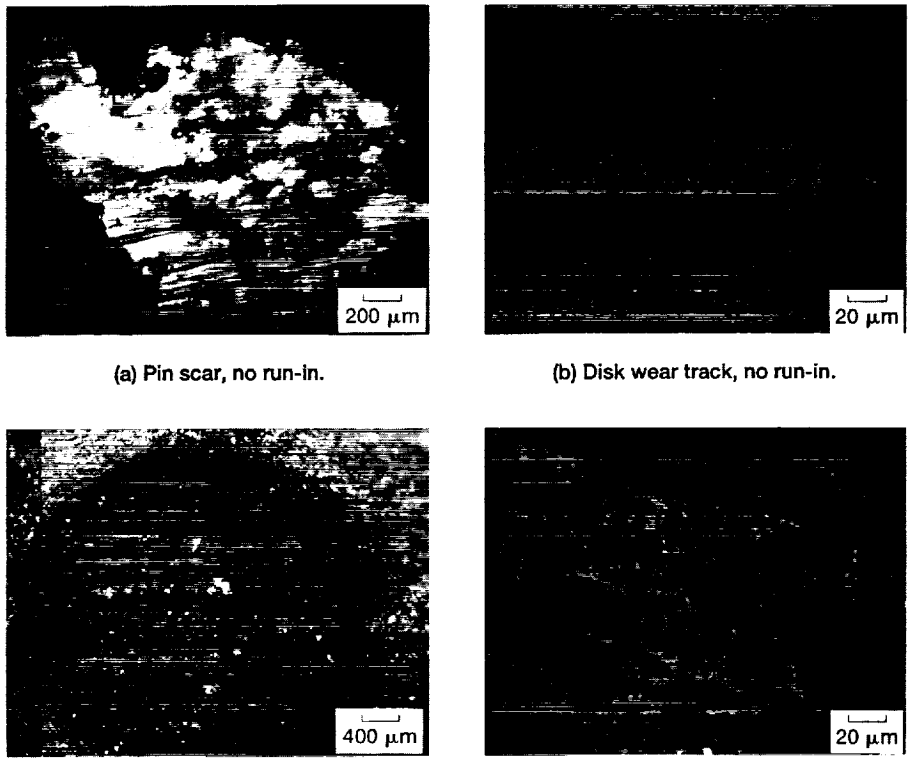

(a) Pin scar, no run-in.

(b) Disk wear track, no run-in.

(c) Pin scar, 0.95 m/s run-in.

(d) Disk wear track, 0.95 m/s run-in.

Figure 4.12.—Wear surfaces of pins and disks from 0.027 m/s tests of HIPped PM212/Au (760 °C).

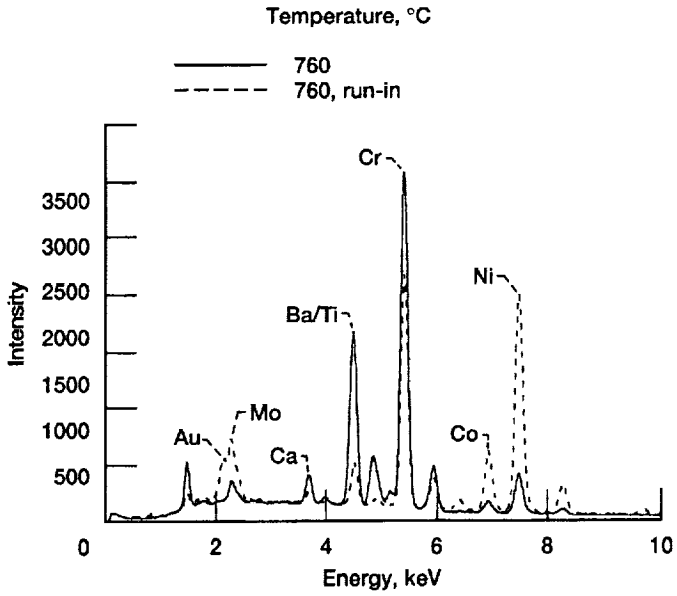

Figure 4.13.—EDS spectra of wear tracks from 0.027m/s tests of HIPped PM212/Au (760 °C).

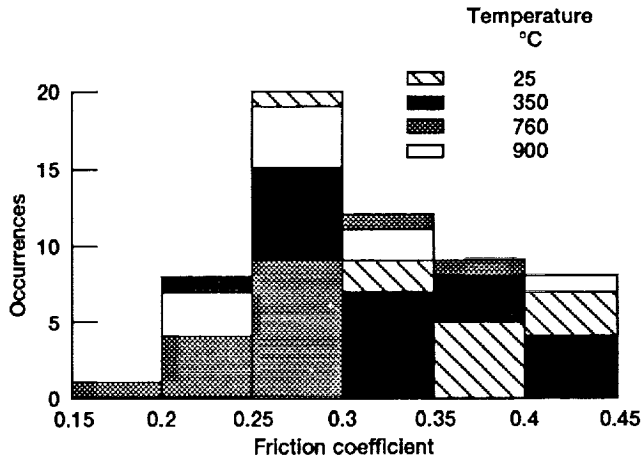

Figure 5.1.—Stacked histogram of average friction coefficients at all temperatures tested for sintered and HIPped alternates.

REPORT DOCUMENTATION PAGE

Form Approved
OMB No. 0704-0188

1. AGENCY USE ONLY (Leave blank)	2. REPORT DATE	3. REPORT TYPE AND DATES COVERED
	November 1992	Final Contractor Report

4. TITLE AND SUBTITLE

Tribological and Microstructural Investigation of the PM200 Series of Self-Lubricating Composites

5. FUNDING NUMBERS

WU-505-63-5A
DE-A101-91CE50306

6. AUTHOR(S)

Michael S. Bogdanski

7. PERFORMING ORGANIZATION NAME(S) AND ADDRESS(ES)

Case Western Reserve University
Department of Mechanical and Aerospace Engineering
Cleveland, Ohio 44106

8. PERFORMING ORGANIZATION REPORT NUMBER

E-7378

9. SPONSORING/MONITORING AGENCY NAMES(S) AND ADDRESS(ES)

National Aeronautics and Space Administration
Lewis Research Center
Cleveland, Ohio 44135-3191

10. SPONSORING/MONITORING AGENCY REPORT NUMBER

NASA CR-190772
DOE/NASA/0030-9

11. SUPPLEMENTARY NOTES

Project manager, Stephen V. Pepper, (216) 433-6061. Prepared under Interagency Agreement DE-A101-91CE50306.

12a. DISTRIBUTION/AVAILABILITY STATEMENT

Unclassified - Unlimited
Subject Category 23
DOE UC-373

12b. DISTRIBUTION CODE

13. ABSTRACT *(Maximum 200 words)*

This master's thesis describes an investigation of the effects of processing and compositional variations on the tribological, microstructural, and compressive strength characteristics of PM212. PM212 is a self-lubricating composite, comprised of a wear resistant metal bonded chromium carbide matrix, containing the solid lubricants barium fluoride/calcium fluoride eutectic and silver. Several alternate composites were formulated which had lubricant and matrix variations. Processing variations included sintering and hot isostatic pressing (HIPping). Pin-on-disk tests were used to screen the alternates for friction and wear properties. Several of the chromium carbide-based self-lubricating composites exhibited low friction and wear in sliding against a nickel-based superalloy. One specific composition contained gold in place of silver to minimize the potential reactivity of the composite with possible environmental contaminants such as sulfur. This formulation also resulted in a composite with good tribological properties. The results indicate that several of these composites have potential use as sliding bearing and seal materials in operation from 25 °C to temperatures as high as 900 °C. The good tribological performance by several different composites showed that the composition of PM212 can be altered without dramatically affecting performance.

14. SUBJECT TERMS

Solid lubricant; Friction; Wear; Composite

15. NUMBER OF PAGES
72

16. PRICE CODE
A04

17. SECURITY CLASSIFICATION OF REPORT	18. SECURITY CLASSIFICATION OF THIS PAGE	19. SECURITY CLASSIFICATION OF ABSTRACT	20. LIMITATION OF ABSTRACT
Unclassified	Unclassified	Unclassified	